Assessment of mixing behaviors of non-Newtonian pseudoplastic fluids in short microdevices

Amar Kouadri [a]*, Embarek Douroum [a,b], Ahmed Ridha El Ouederni [c], Abdelylah Benazza [b], Samir Laouedj [b], Sofiane Khelladi [d].

[a] *Department of Mechanical Engineering, University of Djelfa, Djelfa 17000, Algeria*

[b] *Laboratory of materials and reactive systems, LMSR, Djillali Liabes University, Sidi Bel Abbes 22000, Algeria*

[c] *Research laboratory of Characterizations, Applications and Modelling of Materials (LR18ES08), Faculty of Science of Tunis El Manar, University El Manar, 2092, Tunis, Tunisia*

[d] *Arts et Metiers Institute of Technology, CNAM, LIFSE, HESAM University, F-75013 Paris, France*

***Corresponding author:** amar.kouadri@univ-djelfa.dz (Amar Kouadri)*

Abstract:

Efficient chaotic microdevices have major importance across many potential applications in industrial processes and operations, which form essential parts of microfluidic devices. In microfluidics, The TLCCM micromixer exhibits notable characteristics in terms of mixing of Newtonian fluids which motivated us to compare it with other micromixers using pseudoplastic fluids. The examined micromixers are: L-Shape, OH, and OX. CFD code is utilized to numerically solve Navier-Stokes, the mass conservation and species transport equations. Therefore, the species transport model was selected to analyze the mixing process. The pseudoplastic fluids consist of carboxymethyl cellulose (CMC) solutions, which are characterized using the power-law model, the flow behavior index ranging from 0.49 to 1 and Re_g varies from 0.2 to 70. The effectiveness of mixing was assessed through the mixing degree across various cross-sectional areas. To address this, the analysis encompassed mass fraction contours, velocity profiles, streamlines, flow rates, and the associated mixing energy costs. Our findings report that the TLCCM micromixer presents the elevated mixing degree, where their obtained values vary between 0.80526 and 0.99765. It appears that the occurrence of secondary flows has an additional benefit to improve the mixing performances. Moreover, it requires less mixing energy costs versus other micromixers, where their values vary between 0.00036 and 0.49 Watt.

Keywords: Pseudoplastic behavior; Chaotic advection; Mixing degree; Flow behavior index; Mixing energy cost.

1. Introduction

Microfluidics include both fluid science and engineering systems which studies the design, manufacture and microchannel system operations, and also describe the fluid flows in microdevices with dimensions ranging from millimeters to microns and can process fluid volumes on a microliter scale [1−4]. Unlike traditional fluidic setups, microfluidic systems tend to be much more compact, having dimensions of a few micrometres ranging between tens and hundreds of micrometres. Driving fluid movement across microchannels generally occurs at low flow rates. In this context, the reduced dimensions mean that the viscous forces are predominant in the presence of inertial forces. Consequently, it becomes possible to describe fluid flow at a microscopic scale by flow equations based on a simple proportionality between the flow velocity and the power of the force pushing the fluid [5−11]. Microfluidics has various applications in many biological, medical, chemical and industrial fields [12−20]. Modern uses of microfluidics consist of monitoring and regulating chemical reactions, sample processing, different sensors like flow, pressure and chemical detectors, various actuators such as microvalves, micropumps, microfluidic amplifiers, flow modulation in microsystems like LAC and µ-TAS for biological diagnosis, and DNA examination through polymerase chain reaction, preparation of blood samples to extract DNA, bacteria and virus detection, and ion channel screening…etc [21−31].

Flow within microfluidic devices is frequently employed with low Reynolds numbers, and therefore in the laminar flow regime. This signifies that the flow exhibits stability and that any reduction in the scattering length scales must arise

from complex geometric boundary conditions, not from the instability of the flow, like in the case of various systems of high Reynolds numbers [32, 33]. However, it's evident that laminar flow serves a vital and influential role in fluid mixing. This field has become an active area of research over the past decades, drawing interest and advances from industrial spheres such as microfluidics intended for fluid mixing [34]. The fluid flow in the micromixers takes place within the laminar regime when Reynolds numbers are low due to their reduced dimensions, so the fluid mixing is confronted with a challenge by this. Therefore, for these microfluidic devices, it's indispensable to design and develop micromixers allowing quick and homogeneous mixing but with a low mixing energy cost [35−37]. There are approaches for achieving effective mixing under low Reynolds number conditions. This can be achieved using the physical phenomenon of chaotic advection. In this situation, the secondary flows that stem from the chaotic advection display a significant level of intensity and generate a lot of swirls acting in the microscopic scale on the homogenization, consequently improving the mixing performances [38−40]. All these factors motivate researchers to focus their works and their endeavors on the conception and manufacturing of compact microdevices working in chaotic regime, in particular for non-Newtonian fluids because of their status as the most frequently operated in industry [41−44].

Many works were carried out on Newtonian fluids mixing in different microfluidic devices. While a few studies were conducted on the mixing of non-Newtonian fluids. Most of these works were carried out using active micromixers [45−50], which require outside energy to supply the mixing operation and have a high level of complexity and cost compared to passive micromixers. Moreover, the characteristics or texture of some extremely viscous fluids might be deteriorated by an excessively shearing flow (effect of the blades), as the case of certain biological fluids or polymeric fluids with long molecular chains. In such situations, the use of passive micromixers is a best solution regarding their simple structures and their easy fabrications. In this case, Niederkorn et al. [51] employed the viscosity model of Carreau for characterizing the behavior of non-Newtonian fluids, they showed that the rheological fluids characteristics reduced the velocity of flow. Anderson, et al. [52] also employed Carreau's model to examine the mixing processes of non-Newtonian fluids in periodically stirred 2D and 3D enclosures. The findings were influenced by the rheological fluid properties and stated identical results. Ascanio, et al. [53] employed a model of active mixer to enhance the mixing of pseudoplastic fluids in stirred containers. It was obtained that surrounding the impeller the mixing was enhanced with best mixing quality for low velocities. However, particular attention was spent on using elevated rotating rotors speed to prevent prolonged mixing time and great energy costs. Srisamran, et al. [41] carried out computational investigations employing pseudoplastic fluids to investigate the fluid behavior and fluid mixing in two dimensional, steady, and laminar regimes. The influences of diverse factors including jet inlet Reynolds number between 10 and 200 with flow behavior index ranges between 0.6161 and 1, on the flow behavior and the mixing performances were studied. The mixing temperature was employed as an inert tracer to survey the mixing quality. The power-law model was used by Cho, et al. [54] to define the pseudoplastic fluids rheological behavior. They examined the impacts of different factors on the mixing efficiencies: flow behavior index, undulation amplitude, rippled section length and the intensity of the introduced electric field. Concerning these fluid categories, the authors made a noteworthy observation regarding the enhancement of mixing performance. This enhancement was achieved through two methods: The wave amplitude could be enlarged by making the undulated wall section longer, or by reducing the strength of the electrical field. Tsai et al. [55] investigated the mixing quality of demineralized water solutions and (CMC) solutions within three configurations of micromixer made up of C-shaped components. The micromixer containing C-shaped half-circle elements having a minor centerline radius demonstrated better mixing efficiency compared to the C-shaped micromixer having a large centerline radius. Vortices effectively improved fluid mixing. The 500 ppm CMC solution had a lower average apparent viscosity compared to the 100 ppm CMC solution, so the mixing quality was better for the 500 ppm CMC solution

versus the 100 ppm CMC solution. Afzal, et al. [42] analyzed the fluid flow behaviors and mixing effectiveness of Newtonian and non-Newtonian fluids in a T-junction microfluidic mixer containing one straight channel and one serpentine channel. Water and blood characteristics were considered in the investigation of both Newtonian and non-Newtonian fluids. It was discovered that the serpentine type channel resulted in superior mixing efficiency across all the tested flow rate values, the pressure losses were lower for water compared to blood at equivalent flow rates. Shamsoddini, et al. [56] accomplished a computational study to evaluate the influences of pseudoplastic fluid behavior and the stirrer frequency on the mixing performance of pseudoplastic fluids by using an active model of micromixer with a swinging bar stirrer. The study examined two values of Reynolds number (20 and 72). The study findings illustrated that the active model of micromixer was ineffective for mixing non-Newtonian dilatant fluids. Nevertheless, mixing proves to be more effective and quicker using pseudoplastic fluids, this resulted in a progressive increasing in the mixing index when the flow behavior index increased. Islami, et al. [43] implemented a precise computational analysis on the pseudoplastic fluid mixing, six different curved micromixer geometries were utilized at low values of Reynolds number. Furthermore, their obtained findings illustrate that the geometry of the micromixer didn't significantly affect the mixing of fluids having a flow behavior index near to the value of 1. However, when there's a decrease in the flow behavior index, the influence of the micromixer geometry on the mixing became more pronounced. Their results also provided evidence that the intensity of secondary flows rises with Reynolds number rising, conversely it decreases when the curvature radius increases. Islami, et al. [57] examined the mixing through curved micromixer using the two fluid types in question, Newtonian and non-Newtonian, the used micromixer is characterized by featuring grooves located on the bottom wall. The findings showed the benefit of the implanted grooves in the creation of the chaotic regime and the improvement of the mixing performance without impacting pressure drops. Additionally, grooves angled at 30° provided superior mixing quality across all flow behavior index values tested. Kunti, et al. [58] developed an active micromixer with alternating current electrothermal (ACET) incorporating microgrooves on the bottom of the mixing channel with electrode pairs. Numerical analysis was conducted by characterizing the influence of the apparent viscosity of pseudoplastic fluids (n = 0.6-1.4) on the flow rate and the mixing efficiency. The findings demonstrate that under specific parameters, homogeneous mixing is obtained by rising the flow behavior index. Therefore, the combination of electrothermal forces with passive microstructures in this microfluidic system resulted in better mixing performance for dilatant fluids in comparison with Newtonian and pseudoplastic fluids. Bordbar, et al. [59] conducted a computational analysis to evaluate the efficiency of mixing within modified planar micromixer employing different flow behavior index values between 0.6 and 1.4, the used values of Reynolds number vary between 0.001 and 10.Their findings unveiled that within the examined range of Reynolds numbers, dilatant fluids demonstrate notable mixing performance within the diffusion regime. Whereas, pseudoplastic fluids show good mixing quality for low and high Reynolds number values. Lobasov et al. [60] conducted a computational analysis to evaluate the impacts of fluid rheological behavior on flow patterns and mixing quality within T-junction micromixer. Numerical investigations were conducted for Reynolds number domain of 1 to 250, for three flow behavior index values: 0.3, 0.5, and 0.8. The findings showed that in the symmetric flow regime, mixing quality decreased as the flow behavior index decreased. However, for asymmetric flow regime, mixing was largely unaffected by rheological behavior. He et al. [61] evaluated the mixing capacities of six micromixers defined by split-and-recombine structure composed of E-shaped units. They used Newtonian and pseudoplastic fluids. Their obtained results reveal that the most effective micromixer, named as DBEM-3, achieves exceptional mixing performance, surpassing 0.95 for the overall Reynolds number range (0.5−100), for three values of flow behavior index (0.69; 0.80 and 1). In a computational investigation, Kouadri, et al. [62] assessed the mixing performances within TLCCM micromixer for pseudoplastic fluids, in the case of flow

behavior indices between 0.73 and 1, whereas the Reynolds number values ranging between 0.1 and 50. Elevated mixing performances were found where the mixing degree surpasses 0.96 for the supposed flow behavior index even at low values of Reynolds number. Recently, Kouadri, et al. [63], made a computational analysis to assess the mixing capacity of four passive micromixers. The employed pseudoplastic fluids are the carboxymethyl cellulose solutions, using flow behavior index values ranging from 0.73 to 1. The used generalized Reynolds number ranges between 0.1 and 50. The results of their investigation demonstrate that the TLCCM micromixer exhibits the best mixing degrees that reach 0.96 across the entire generalized Reynolds number values and the flow behavior index under examination. Moreover, it exhibits a reduced mixing energy cost against the other considered micromixers. This study particularly focuses on non-Newtonian fluid mixing exhibiting pseudoplastic behavior in a short TLCCM micromixer after proving its great capacities for Newtonian fluid mixing [64−66]. Previous work has shown that high mixing performance for non-Newtonian fluids can be achieved at low Reynolds numbers when using long micromixers (more than 7.5 mm). Motivated by these considerations, we are interested in the mixing efficiency evaluation of pseudoplastic fluids in a short TLCCM micromixer (*l*/W=1) with reduced length of 3.75 mm, exclusively in the laminar regime using ANSYS Fluent code to characterize the pseudoplastic fluids mixing. In order to confirm its superiority, the TLCCM micromixer with (*l*/W=1) was compared with potential microdevices that were further studied (L-shape, OH, and OX). The impacts of the flow behavior index, the generalized Reynolds number, and the geometry wall effects on the pseudoplastic fluids mixing are presented and analyzed.

2. Micromixer geometrical models

Four geometric models have been studied, the main dimensions are shown in Fig. 1, which highlights different details of the studied micromixers, and along them the mixing quality is evaluated. Fig. 1(a) shows a three-dimentional view of the TLCCM micromixer showing two entrances and exit. The different dimensions of this micromixer are illustrated, such as: the channel width W, the height of each layer d, the micromixer width H, the width of the transversal channel b, the step S, and the length of each mixing unit (b + S), are respectively: 300 µm , 150µm, 1070µm, 150µm, 640µm, 790µm. The entrances and the exit section dimensions are: 150 × 300 µm and 300 × 300 µm, and the entire length of the micromixer is 3750 µm.

The hydraulic diameter is defined by: $D_h = \frac{2d \cdot W}{d + W}$

To demonstrate the efficiency of the TLCCM micromixer, for the context of the pseudoplastic fluids mixing, against those studied recently, three micromixers are designed with the same value of the hydraulic diameter (200 µm) and also the same equivalent total length which equal to (3750 µm). Fig.1 (b), (c), and (d) illustrate respectively the perspective view of the proposed micromixers: L, OH, and OX, with their dimensions.

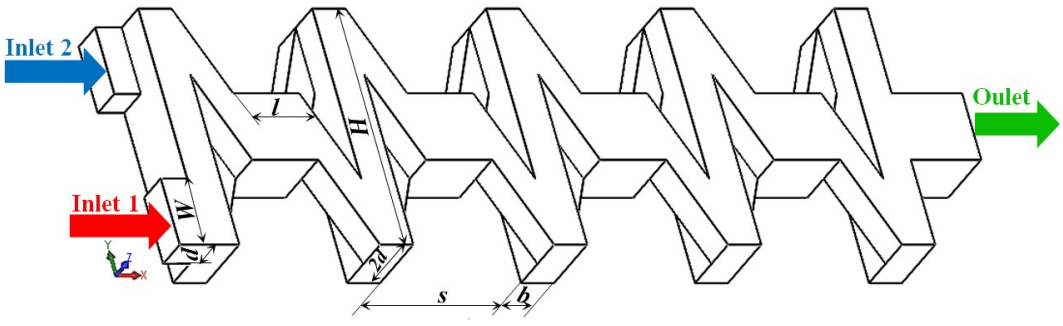

(a)

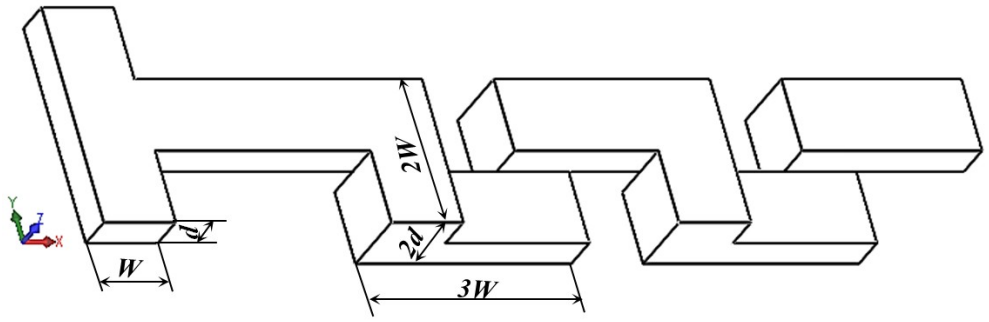

(b)

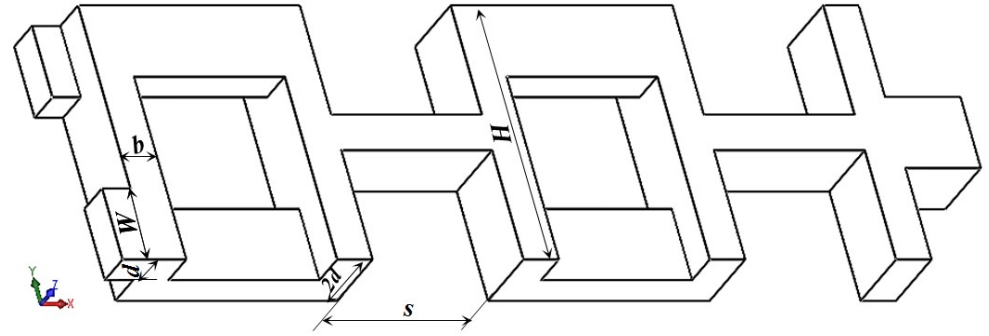

(c)

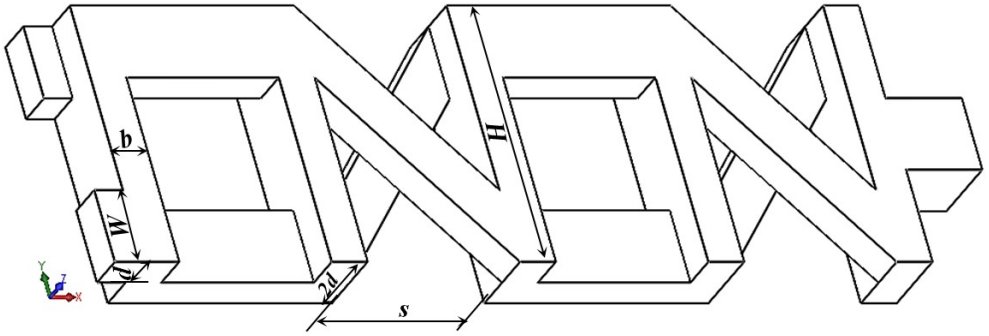

(d)

Fig. 1. Description of considered micromixers: (a) TLCCM; (b) L-Shape; (c) OH-Shape; (d) OX-Shape.

3. Mathematical models and numerical approaches

This section outlines the main equations and the associated boundary conditions that govern the system, including the generalized Reynolds number expression and all parameters used to evaluate the mixing performance. Also, the appropriate mixing model selected for analysis is delineated.

3.1. Mathematical models

The computational simulations have been conducted employing ANSYS Fluent code. The equations that govern incompressible and steady flows in three dimensions consist of the continuity equation (Eq 1 and 2), and the momentum equations involving the tensor of shear stress (Eq 3, 4, 5, and 6). Expressing these equations, we have:

$$\nabla . \vec{V} = 0 (1)$$

which can be developed as follows:

$$\frac{\partial u}{\partial x} + \frac{\partial v}{\partial y} + \frac{\partial w}{\partial z} = 0 (2)$$

$$\rho(\vec{V}\cdot\nabla)\vec{V}=-\nabla P+\nabla\cdot\acute{\tau}(3)$$

Its expanded notation is expressed by:

$$\left(u\frac{\partial u}{\partial x}+v\frac{\partial u}{\partial y}+w\frac{\partial u}{\partial z}\right)=\frac{-1}{\rho}\frac{\partial P}{\partial x}+\frac{1}{\rho}\left[\frac{\partial \tau_{xx}}{\partial x}+\frac{\partial \tau_{xy}}{\partial y}+\frac{\partial \tau_{xz}}{\partial z}\right](4)$$

$$\left(u\frac{\partial v}{\partial x}+v\frac{\partial v}{\partial y}+w\frac{\partial v}{\partial z}\right)=\frac{-1}{\rho}\frac{\partial P}{\partial y}+\frac{1}{\rho}\left[\frac{\partial \tau_{yx}}{\partial x}+\frac{\partial \tau_{yy}}{\partial y}+\frac{\partial \tau_{yz}}{\partial z}\right](5)$$

$$\left(u\frac{\partial w}{\partial x}+v\frac{\partial w}{\partial y}+w\frac{\partial w}{\partial z}\right)=\frac{-1}{\rho}\frac{\partial P}{\partial z}+\frac{1}{\rho}\left[\frac{\partial \tau_{zx}}{\partial x}+\frac{\partial \tau_{zy}}{\partial y}+\frac{\partial \tau_{zz}}{\partial z}\right](6)$$

In compact notations, the quantities V, ρ, P and $\acute{\tau}$ denote in the respective order: the fluid velocity, the fluid density, the static pressure, and the tensor of shear stress.

For equations (Eq 4, 5, and 6), τ_{ij} represents the viscous tensor of shear stress. For a pseudoplastic fluid and according to the power-law model, this tensor is written in the form:

$$\tau_{ij}=\mu_{app}\varepsilon_{ij}(7)$$

where μ_{app} and ε_{ij} represent respectively the apparent viscosity and the strain rate tensor, which is expressed as:

$$\varepsilon_{ij}=\frac{\partial u_i}{\partial x_j}+\frac{\partial u_j}{\partial x_i}(8)$$

To describe the viscosity of pseudoplastic fluids ($n<1$), the behavior of the fluids through a restricted interval of shear rates is better represented by the power-law model (Ostwald De-Waele) compared to other models. It's frequently used in various research works because of its simplicity.

$$\tau=m\dot{\gamma}^{n}(9)$$

Whereas "m" represents the coefficient of the fluid consistency and "n" denotes the flow behavior index, so the apparent viscosity can be given by:

$$\mu_{app}=m\dot{\gamma}^{n-1}(10)$$

where $\dot{\gamma}$ represents the shear rate which is given by:

$$\dot{\gamma}=\sqrt{\frac{(\varepsilon_{ij}:\varepsilon_{ij})}{2}}=\sqrt{\frac{I_2}{2}}(11)$$

With I_2 denotes the second invariant of the strain rate tensor. And the apparent viscosity μ_{app} can be linked to this second invariant by the following relation:

$$\mu_{app}=m\left(\frac{I_2}{2}\right)^{\frac{n-1}{2}}(12)$$

with :

$$\frac{I_2}{2}=2\left(\frac{\partial u}{dx}\right)^2+2\left(\frac{\partial v}{\partial y}\right)^2+2\left(\frac{\partial w}{\partial z}\right)^2+\left(\frac{\partial u}{\partial y}+\frac{\partial v}{\partial x}\right)^2+\left(\frac{\partial u}{\partial z}+\frac{\partial w}{\partial x}\right)^2+\left(\frac{\partial v}{\partial z}+\frac{\partial w}{\partial y}\right)^2(13)$$

ANSYS Fluent provides various models for characterizing mixing. The species transport model is frequently employed in the fluid mixing by considering the mass diffusion coefficient.

To simulate the fluid mixing and the species transport, the CFD code solves the conservation equations involving convection and diffusion terms for every individual species. Since for all species "*i*", the total of the mass fractions is equal to 1.

The fluid species conservation equation is given by:

$$\nabla \cdot \left(\rho V C_i \right) = - \nabla \cdot J_i \quad (14)$$

where J_i is the flux of mass diffusion for fluid species. This flux is a function of concentration gradients and pressure gradients that induce the diffusive motion during mixing. The dilute approximation (according Fick's law) is included in the computational code to model the mass diffusion.

The mass diffusion flux is expressed by:

$$J_i = - D_i \nabla \left(\rho C_i \right) \quad (15)$$

where D_i denotes the coefficient of mass diffusion for species "i" within the mixing process.

Therefore, the equation of species transport is expressed by:

$$\left(V \cdot \nabla \right) C_i = D_i \nabla^2 C_i \quad (16)$$

This equation is written in Cartesian coordinates using the following expanded notation:

$$u \frac{\partial C_i}{\partial x} + v \frac{\partial C_i}{\partial y} + w \frac{\partial C_i}{\partial z} = D_i \left(\frac{\partial^2 C_i}{\partial x^2} + \frac{\partial^2 C_i}{\partial y^2} + \frac{\partial^2 C_i}{\partial z^2} \right) \quad (17)$$

The diffusion coefficient D_i is supposed to be 3.6×10^{-10} m^2/s for the pseudoplastic fluids case (Das, et al. [67]). Moreover, the mixing process is controlled by the mechanism of chaotic advection.

The imposed boundary conditions are:

- A non-slip condition on the walls is considered, where the velocity components are: U=V=W=0.
- For the two fluid inlets, uniform velocities are imposed: $U = C^{te}$.
- The mass fraction of fluid 1 at inlet 1 equal to 1 and that of inlet 2 equal to 0, and the reverse for fluid 2.
- An atmospheric pressure at the outlet.

3.2. Fluid characteristics

For the pseudoplastic fluid flows, the used fluid is the CMC solutions. Their density proposed by Srisamran et al. [41] is supposed to be 1000 kg/m^3. The CMC solutions rheological properties such as: the coefficient of consistency and the flow behavior index are specified in table 1.

Table 1. Rheological behaviors of CMC solutions according to Fellouah, et al. [68], and Pinho et al. [69]

CMC (%)	n (-)	m ($Pa.s^n$)
0	1	0.000902
0.1	0.93	0.0066
0.2	0.85	0.0252
0.25	0.75	0.097
0.7	0.49	2.75

3.3. Mixing characterization

For quantifying the hydrodynamic mixing efficiency of the proposed micromixers, the mixing degree (D_m) is expressed by:

$$D_m = 1 - \frac{\sigma}{\sigma_0} \quad (18)$$

with σ denotes the standard deviation of the average mixing concentration in a transversal plane, which is obtained by the included function of the CFD code post processing:

$$\sigma^2=\frac{1}{N}\sum_{i=1}^{N}\left(C_i-\overline{C}\right)^2 (19)$$

The maximum standard deviation is taken as the highest value for non-mixed fluids and the lowest value for fully mixed fluids. Here, *N* presents the overall number of cells in a transversal section, and $\overline{C}$ represents the mean concentration. The mixing process is considered homogeneous when the values of the mass fraction of both fluids are equivalent (the two equal 0.5).

The equation used to derive the maximum value for standard deviation within the data parameters is:

$$\sigma_0^2=\overline{C}\left(1-\overline{C}\right) (20)$$

The mixing degree: D_m = 1 denotes a perfectly mixed state (σ = 0), while D_m = 0 denotes a non-mixed case (σ = σ_0). High D_m value signifies a concentration that is more uniform and indicates improved mixing efficiency.

3.4. Generalized Reynolds number expression

It's imperative to define the nature of the flow, because this defines the dominant phenomena. The main criterion for predicting the nature of the flow regime is the Reynolds number. The Reynolds number denotes the ratio between the inertial and the viscous forces.

For pseudoplastic fluids, the viscosity varies with the strain rate. It's crucial to formulate a generalized Reynolds number expression that incorporates the rheological behaviors of the fluid. In the case of any sections (circular, rectangular, elliptical, etc.), several expressions of the generalized Reynolds number have been developed in the literature. However, Delplace et al. [70] have proposed an expression of the generalized Reynolds number that uniquely applies to both Newtonian and pseudoplastic fluids within a rectangular cross-section, irrespective of the aspect ratio. Employing this expression enables meaningful comparisons while altering the flow behavior index and the geometry under investigation. The generalized Reynolds number is expressed by:

$$\Re_g=\frac{\rho\bar{u}^{2-n}D_h^n}{m\left(\left(24n+\xi\right)/\left(24+\xi\right)n\right)^n\xi^{n-1}} (21)$$

where $\bar{u}$is the average velocity of flow, while ξ represents the nondimensional geometric parameter.

Table. 2. The geometric coefficient ξ in dependency with different values of aspect ratio $\alpha^{¿}$.

$\alpha^{¿}$	0.25	0.5	0.75	1.0
ξ	9.116	7.774	7.238	7.113

In our case, the selected geometric coefficient ξ depends to an aspect ratio $\alpha^{¿}$ as follows: $\alpha^{¿}=\frac{d}{W}=0.5;\ \xi=7.774.$

3.5. Computational procedure

Inside this part, we outline the numerical methodology, detail the chosen numerical approach, elaborate on the employed numerical discretization scheme, and present the mesh independency analysis conducted to determine the appropriate mesh grid for the considered micromixers.

3.5.1 Numerical approach of discretization method

In this study, the second-order discretization method is selected to achieve concrete findings with less computation time. To validate the precision and reliability of the numerical predictions for mixing performance, a second-order upwind scheme is employed to discretize the convection terms in the momentum and species transport equations. Since

convergence is dependent on the pressure-velocity coupling, we applied the SIMPLEC algorithm to obtain a converged and stable solution. Moreover, the pressure correction is guaranteed through the use of under-relaxation factors set at 0.3, which helps accelerate convergence. The iterative calculations convergence was obtained when the residuals value is lower than 10^{-6}.

3.5.2 Mesh independency analysis

To evaluate the independency of the results with the mesh refinement for determining the optimal cell size, an unstructured and a uniform mesh consisting of tetrahedral cells are used (Fig. 2). Also, four grid meshes in the micromixer (l/W = 1), ranging from 221 × 10^3 to 1068 × 10^3 were tested. In this study, the generalized Reynolds number stands at 50, accompanied by a flow behavior index of 0.49. For that, the local mixing degree is plotted along the mixing channel for the different mesh grids. It can be seen that the mixing degree for the mesh grids (637 × 10^3 and 1068 × 10^3) are confused. Table. 3 shows the relative error values between each mesh grid compared to the 1068 × 10^3 cell grid. The lowest error values were obtained with the 637 × 10^3 cell grid, indicating it was optimal. Therefore, the grid with 637 × 10^3 cells was selected. Furthermore, according to the findings of the independency analysis, the 637× 10^3 cell grid equivalent to 16 µm of cell size, is refined sufficiently to obtain precise results with less calculation time.

As asserted by the sensitivity test, different grids with the optimal size were used to generate meshes for the other micromixers, as indicated in the Fig. 3. For the two micromixers TLCCM and OX, which present acute angles, a tetrahedral-based unstructured and uniform mesh was generated. While, for the remaining two micromixers L and OH, a structured mesh with hexahedral elements, maintaining uniformity, was employed.

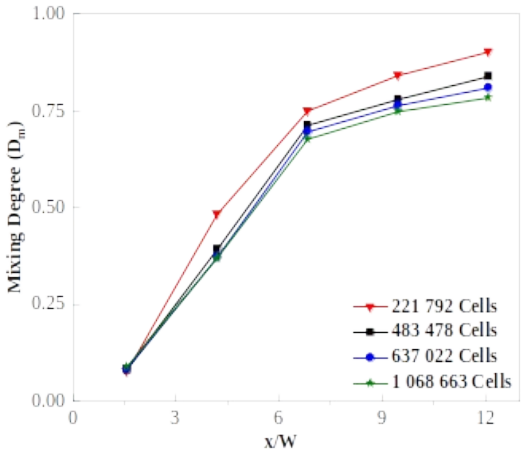

Fig. 2. Mesh independence study of mixing degree evolution in a TLCCM micromixer for pseudoplastic fluids with flow behavior index of n = 0.49 and generalized Reynolds number of Re_g = 50.

Table. 3. Mixing degree errors compared to the 1 068 663 Cell grid.

	Errors (%)		
Sections	**221 792 Cells**	**483 478 Cells**	**637 022Cells**
P_1	13.89244386	6.415770841	8.133130059
P_2	30.64039402	6.150745802	0.689132279
P_3	10.79917056	5.304706528	2.792223686
P_4	12.45827547	4.183572083	2.093637250

Exit	15.12325671	7.031153707	3.264096471

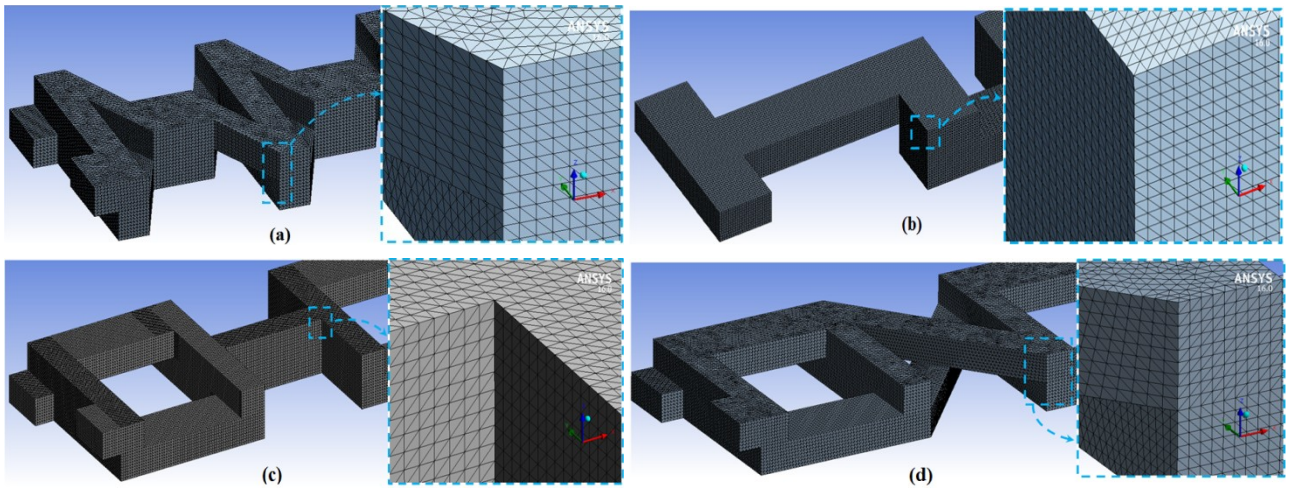

Fig. 3. Mesh grids generated for different micromixers with zoomed views: (a) Two-Layer Crossing Channels Micromixer (l/W=1), (b) L-Shape micromixer, (c) OH-Shape micromixer, and (d) OX-Shape micromixer.

4. Results and analysis

To achieve better mixing for non-Newtonian fluids, the potential chaotic micromixers that have been investigated previously for Newtonian fluids are examined in this study to evaluate their hydrodynamic performances. The influences of the Reynolds number, the flow behavior index, and the micromixer geometry on the mixing of pseudoplastic fluids are presented and analyzed.

4.1. Assessing the CFD code accuracy

Validation simulations were conducted to check the accuracy of the CFD code. The results were quantitatively compared with previous findings reported by Tsai et al. [55] concerning the mixing degree, the working fluids are CMC solutions with a flow behavior index of (n=0.8229). Fig. 4(a) illustrates the progression of the mixing degree at the outlet of each pattern of C for a generalized Reynolds number of 15.849 in the micromixer SCSM-90/34. Moreover, the curves exhibit close alignment, with a maximum relative error of 12.47%. In Fig. 4(b), the mixing degree is calculated at the micromixer outlet for generalized Reynolds numbers ranging between 0.0215 and 57.761. The two curves follow nearly identical trends and align closely, with only a very small noticeable difference. The distinction among the different evolutions stays within the numerical technique's precision range.

A qualitative assessment has been performed utilizing the Simple Curved micromixer (SC) used by Islami et al. [57]. Fig. 5 depicts the mass fraction spreads within the mid-planes and at the outlet for a generalized Reynolds number value of 0.1, considering two flow behavior indices, 0.6 and 1. The figure demonstrates a high degree of similarity in mass fraction distributions, affirming the comparability of our results. As a result, the validation test has been demonstrated.

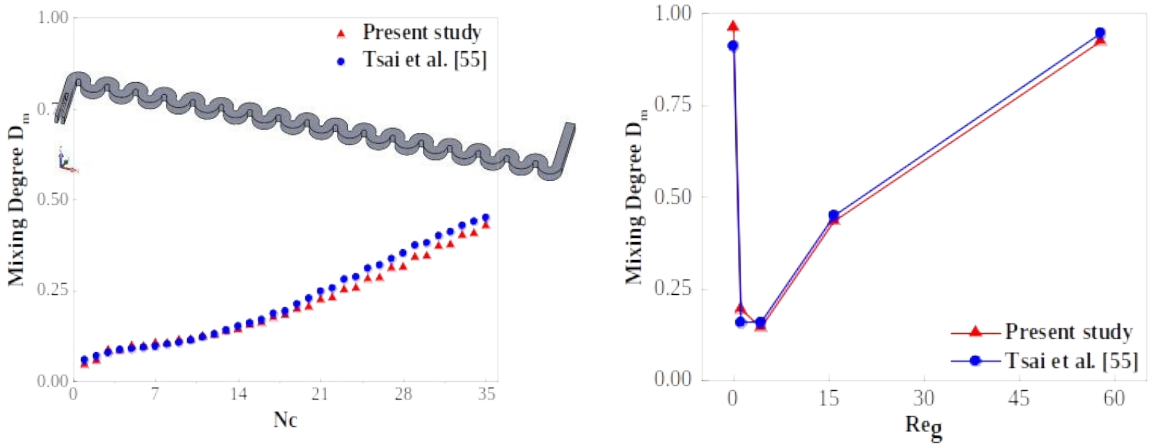

Fig. 4. Quantitative validation of our numerical results against previous results by Tsai et al. [55] for non-Newtonian fluid (n=0.8229) at Re_g=15.849: (a) Progression of mixing degree at the exit of each C-shaped pattern, (b) Variation of mixing degree versus the generalized Reynolds number.

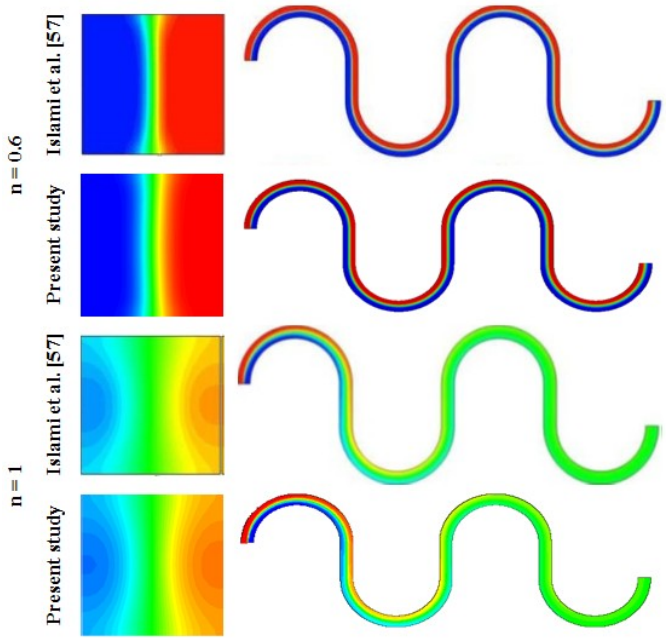

Fig. 5. Qualitative validation of our numerical findings against previous works for non-Newtonian and Newtonian fluids mixing using the Simple Curved micromixer (SC) of Islami et al. [57], at generalized Reynolds number of Re_g = 0.1.

4.2 Hydrodynamic characteristics and secondary flow patterns within the micromixer (*l*/W = 1)

To illustrate the effect of the secondary flows generated within the micromixer with (*l*/W = 1) on the mixing performances, it's interesting to present qualitatively the flow velocity contours and the velocity vectors in different cross-section planes of the micromixer last unit (Fig. 6(a)). For low value of generalized Reynolds number (Re_g = 1), we can see in Fig. 6(b) that for Newtonian (n=1) and non-Newtonian (n= 0.49) fluids, the flow structure is almost identical in terms of velocity vector distributions in all sections despite the observed difference in velocity values. This can be attributed to the specific flow regime which is characterized by molecular diffusion (creeping flow).

In dynamical systems theory, flows have a complex structure if the phase space contains one or more unstable elements. The hyperbolic points represent the unstable elements located in the phase space. The area surrounding an elliptical

point forms an obstacle which disfavors the mixing, In the case of a hyperbolic point, there are two local behaviors associated with it corresponding to the physical directions of compression and stretching that appear clearly in the entrance and exit of the crossing elongation (Fig. 6(b) and (c)). This behavior denotes a significant indication of the emergence of chaotic advection regime, especially for the higher Reynolds number value (Re_g = 70). In all cross-sectional planes of the elongation, the interface of fluid becomes compressed along the diagonal axis at the intersecting inlets, while that on the other diagonal line in the crossing outlets is stretched, as indicated by the orientation of the velocity vectors in both Newtonian and non-Newtonian fluids, this phenomenon of compression and stretching represents one of the fundamental mechanisms for enlarging the interfacial layer between fluids, which enhances the mixing efficiency. Consequently, the intense flow patterns at the crossing elongations yielded exceptional mixing efficiency for the TLCCM micromixer. Moreover, the flow structure in Fig. 6(c) is completely different compared to the molecular diffusion regime (Re_g = 1), it also exhibits variation based on the flow behavior index within the chaotic advection regime (Re_g = 70). The intensity of the secondary flow for Newtonian fluids increases at Re_g = 70, which is reflected by the appearance of vortex structures in all sections, particularly in the mid-plane of the elongation. The occurrence of the chaotic advection phenomenon at Re_g = 70 favors clearly the mixing quality of Newtonian fluids where the agitation becomes easier.

(a)

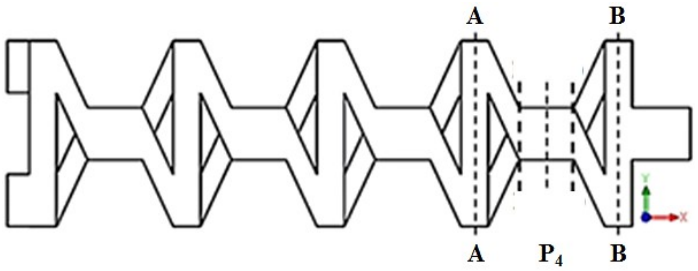

(b)

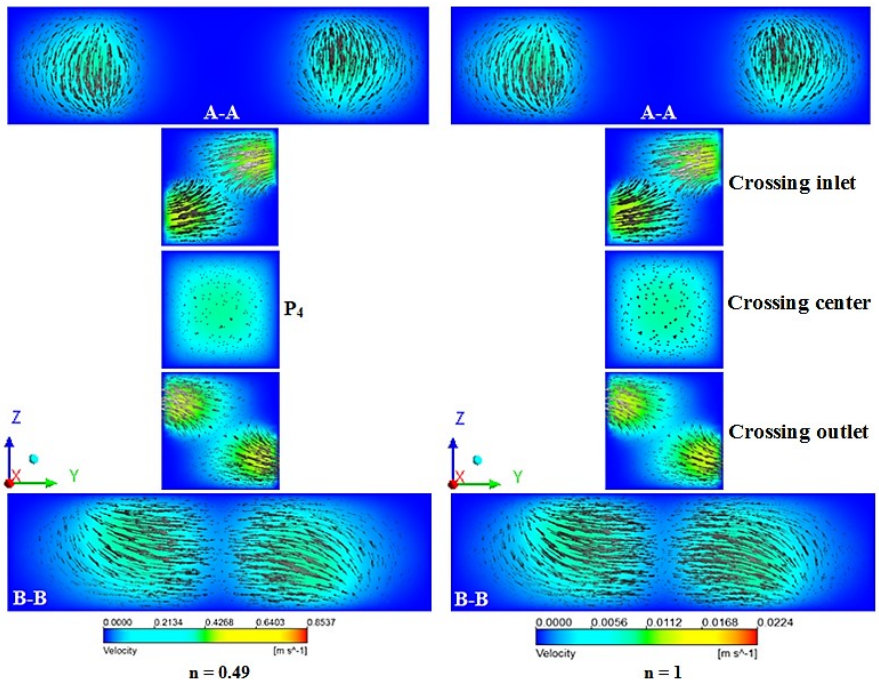

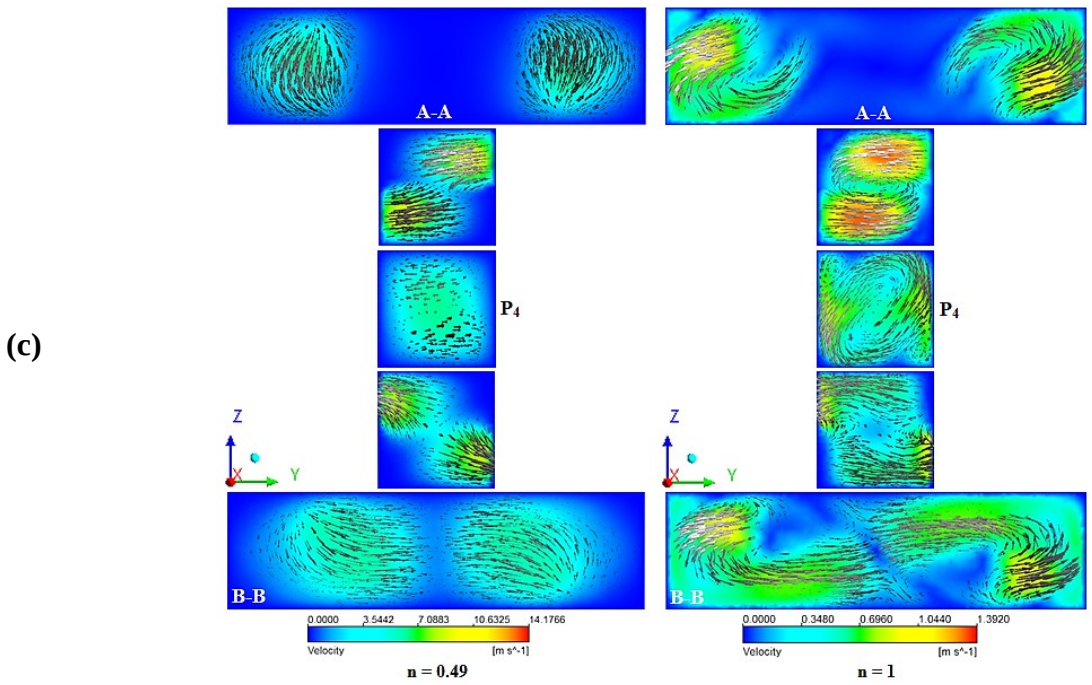

Fig. 6. (a) Cross-sectional planes positions, **(b** and **c)** Contours and velocity vectors at cross-sectional planes of the last unit of the TLCCM micromixer for Newtonian (n = 1) and non-Newtonian fluids (n = 0.49): **(b)** Re_g = 1, **(c)** Re_g = 70.

It's known that the apparent viscosity of pseudoplastic fluids is reliant on different factors, which are the shear rate, the flow behavior index, the consistency coefficient, and the generalized Reynolds number. From Table 1, it's clear that the consistency coefficient varies with the flow behavior index values. Fig. 7 shows the variation of the apparent viscosity throughout the y axis at the exit for two generalized Reynolds number values (Re_g = 1 and 70) over the range of the flow behavior index (n = 0.49; 0.75; 0.85; 0.93; and 1). It's clear that the apparent viscosity varies inversely with the flow behavior index. Non-Newtonian fluids have higher apparent viscosity values which disadvantages mixing because the agitation becomes more difficult. In contrast, Newtonian fluids have low values which promote mixing where the agitation becomes easier.

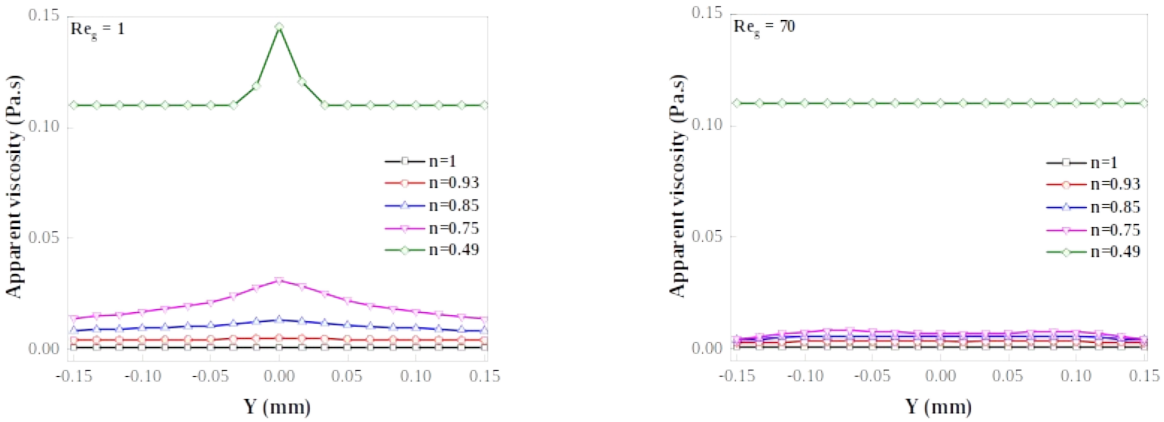

Fig. 7. Variations of the apparent viscosity on the meridian axis at the exit of TLCCM Micromixer (*l*/W=1).

Fig. 8 demonstrates the shear rate curves on the mid-line at the TLCCM Micromixer outlet plane for various flow behavior index values. It can be seen that the highest shear rates are found beside to the micromixer walls, in particularly for low flow behavior index values (n = 0.49), which is related to the shear thinning fluids. However, the

lowest shear rates are observed for Newtonian fluids (n = 1). The shear rate on the middle zone is lower than that on the walls, it increases from the center to the side of the walls. For shear-thinning fluids, decreasing the shear rate locally is beneficial to enhance the mixing quality. When the fluid viscosity is reduced locally, the local velocity is decreased, which leads to the increase in the residence time, therefore, the mixing becomes more homogeneous. However, the impact of the shear rate on the fluid dynamics is almost significant.

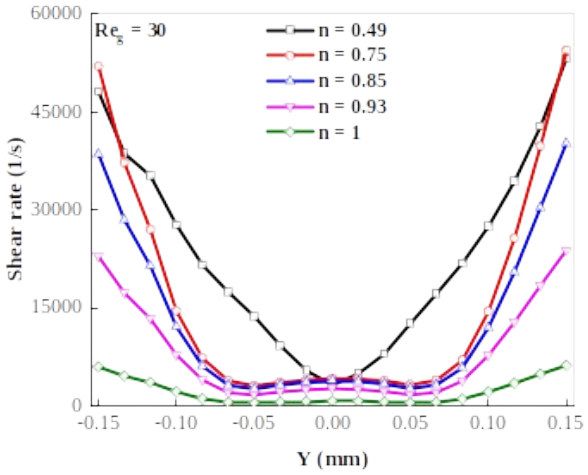

Fig. 8. Shear rate curves on the mid-line at the outlet plane of TLCCM Micromixer (*l*/W=1) for different flow behavior index values.

To show the influence of the secondary flows generated in the elongations, it's necessary to represent the velocity curves in the middle of the last crossing. It's known that through the generalized Reynolds number augmentation, the vortices created at the transversal sections are strong and possess distinct structures [54]. The entanglement of streamlines and the flow ascending and descending are expressed by the tangential (Vz) and radial (Vy) velocity curves, as illustrated in Fig. 9. The velocity curves in the mid-plane of the last crossing are represented for two values of the generalized Reynolds number (Re_g = 1 and 70). This figure shows that the velocity varies inversely with the flow behavior index. The Newtonian fluid has reduced velocity values for the two considered Reynolds numbers than the non-Newtonian fluids. At Re_g=1 the shear thinning fluid (n = 0.49) has high velocity values which decrease as n increases to reach relatively low values for the Newtonian fluid (n = 1). We also note that the tangential velocity component ascends along one side while it descends along the opposite side with respect to the horizontal center line, and directed in two opposite directions according to the vertical meridian line, this behavior explains the fluids rotation when they cross through the crossing elongation. The comparison between the velocity components values shows that the radial velocity component is relatively higher than the tangential component, this superiority is due to the fluid jets which come from the two upper and lower layers.

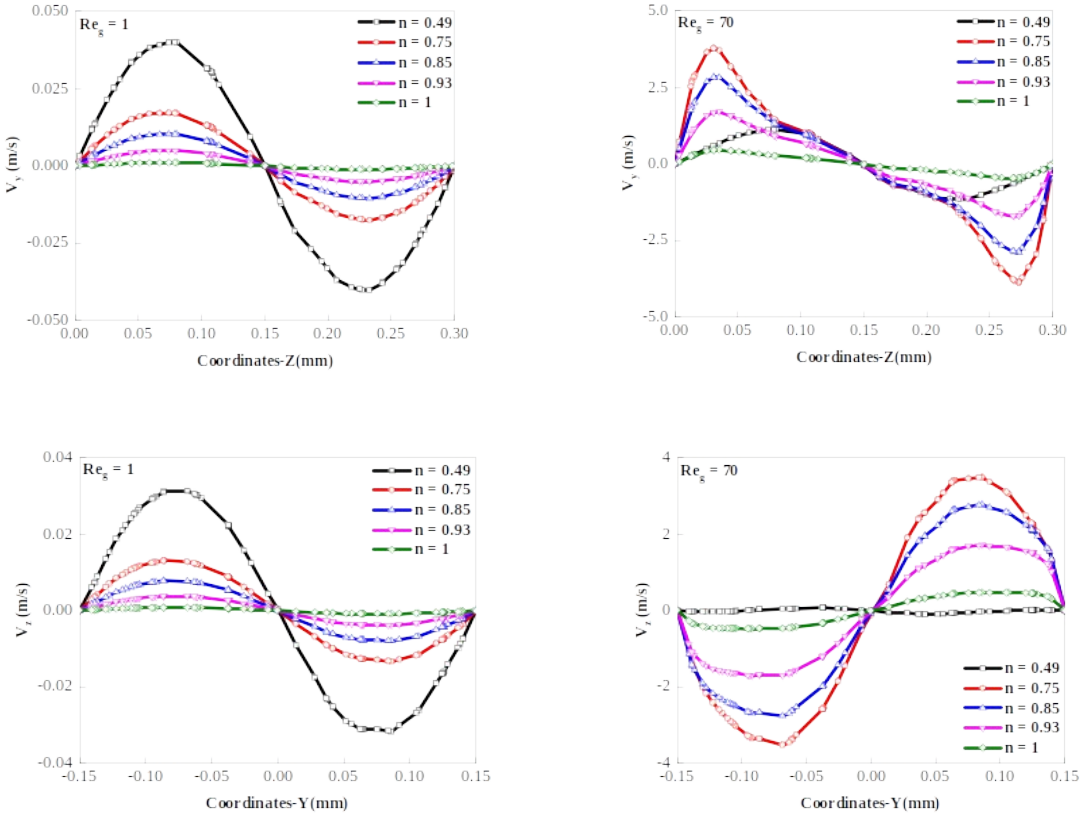

Fig. 9. Velocity curves throughout the mid-line of the last crossing elongation of TLCCM Micromixer (*l*/W=1) for various flow behavior index (0.49, 0.75, 0.85, 0.93 and 1), for Re_g = 1 and Re_g = 70.

Fig. 10 presents the evolution of the radial velocity curves (Vy) and the tangential velocity curves (Vz) throughout the TLCCM micromixer for different flow behavior index values and for two values of generalized Reynolds number. It's evident that the velocities have almost zero values outside the micromixer crossing zones, and it's clear that the secondary flows are created in the crossing elongation zones, where the velocities take on non-zero values. The velocities also vary according to the flow behavior index, so the strength of the secondary flow varies with the flow behavior index. For the pseudoplastic fluid with n = 0.49 and Re_g = 70, the primary flow is more dominant compared to the secondary flows which explains the decrease in the values of the radial and the tangential velocity components.

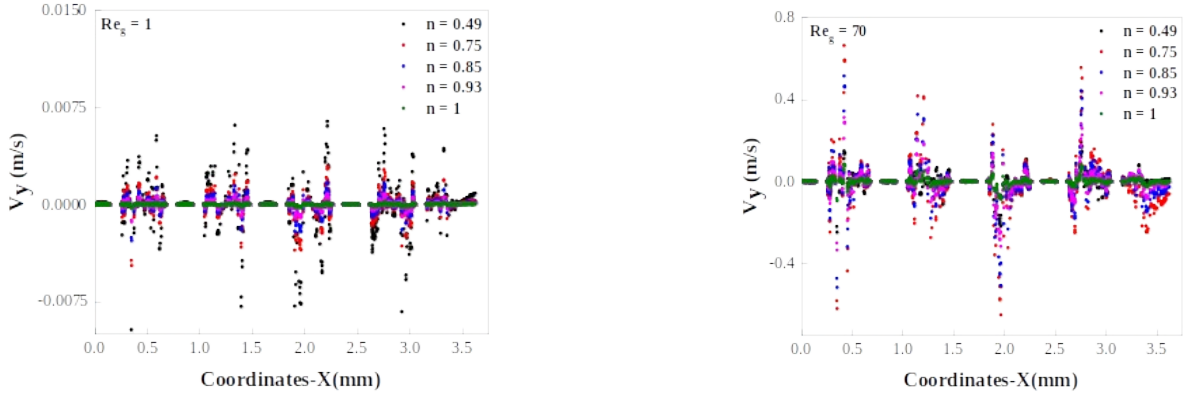

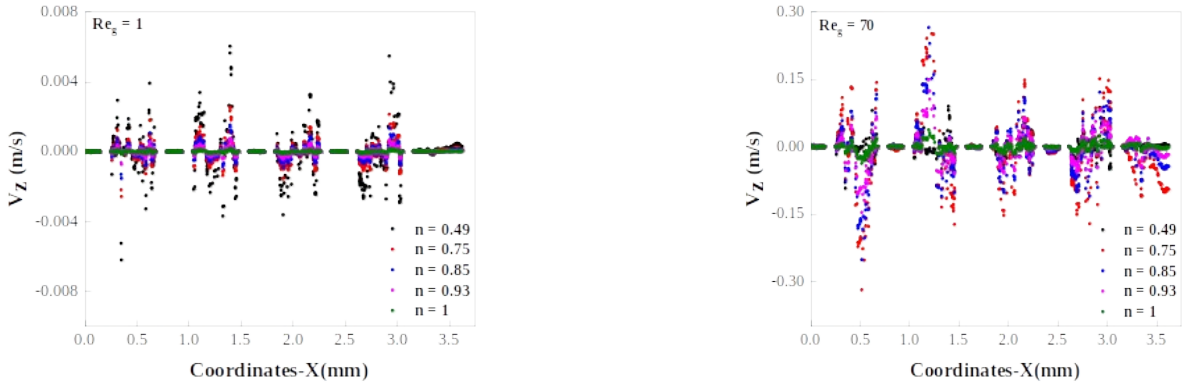

Fig. 10. Velocity curves throughout the mid-height of the TLCCM micromixer (*l*/W=1), for various flow behavior index (0.49, 0.75, 0.85, 0.93 and 1), for Re_g = 1 and Re_g = 70.

The objective of achieving uniform mixing with fast and efficient transport is noteworthy. Nevertheless, these objectives often counteract each other due to the conflict between a high flow rate and the necessary residence time for effective mixing. The interplay between these factors is complex: a high flow rate limits the time available for adequate mixing, and conversely, aiming for thorough mixing may necessitate a lower flow rate. The mixing degree variations versus the flow rate in relation to the flow behavior index at the micromixer outlet are depicted in Fig. 11. This figure illustrates a vast spectrum of the mixing degrees and the flow rates across a range of flow behavior indices spanning from 0.49 to 1. Within this range, the flow exhibits significant diversity for identical Reynolds number values. For instance, at Re_g = 0.2, the flow rate of the pseudoplastic fluid (n = 0.49) exceeds the flow rate of the Newtonian fluid (n = 1) by 66 times. As illustrated previously, the Newtonian fluid presents lower velocity values against the non-Newtonian fluid, which explains the decrease in flow rate as the flow behavior index rises. In contrast, the mixing degree rises as the flow behavior index climbs for all the considered values of the generalized Reynolds number. According to this figure, the pseudoplastic fluid is characterized by a high flow rate and therefore a short residence time but it has a relatively low mixing degree compared to the Newtonian fluid which is distinguished by a low flow rate and therefore an extended residence time.

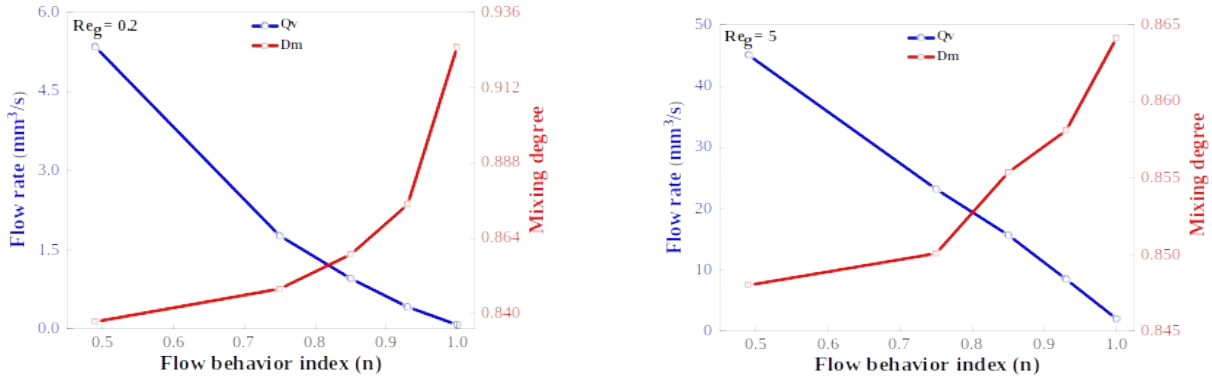

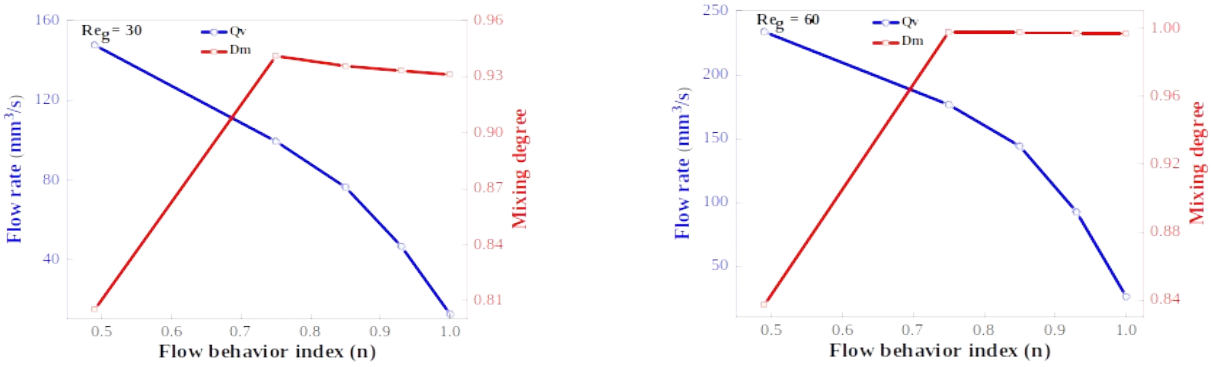

Fig. 11. Mixing degree and flow rate variations with different flow behavior index (0.49, 0.75, 0.85, 0.93 and 1) at the exit of the TLCCM micromixer for generalized Reynolds numbers of (0.2, 5, 30, and 60).

4.3. Flow patterns in the studied micromixers

In this part, a comparison of the mixing performances was performed out between the TLCCM micromixer and other considered micromixers (L, OH, and OX). Fig. 12 and 13 present the distribution of mass fraction contours and streamlines in the studied micromixers for two considered values of flow behavior index n=1 and n=0.49 and three generalized Reynolds numbers (Re_g = 1, 30, and 70). The flow pattern and mixing quality are similar for all micromixers in the case of creeping flows (Re_g = 1). While, for high Reynolds number values (Re_g = 30 and 70), a substantial increase in mixing efficiency is detected particularly for the TLCCM and L micromixers, with the appearance of vortex structures illustrated by streamlines. Clearly, the introduction of crossing elongations within the TLCCM micromixer facilitates the formation of stretching and compression patterns within the transversal sections. This phenomenon contributes to achieving a more uniform mixing. These structural patterns serve a crucial role throughout the mixing procedure. It's also observed an occurrence of twisted structures that form in the elongation zones of the TLCCM micromixer for the Newtonian fluids which disappear for the non-Newtonian fluids (n = 0.49). The complex configuration of the TLCCM micromixer defined by the division-recombination and the elongation of the crossing strongly favors the chaotic advection in comparison to the other micromixers, which present a weak intensity of the chaotic advection phenomenon.

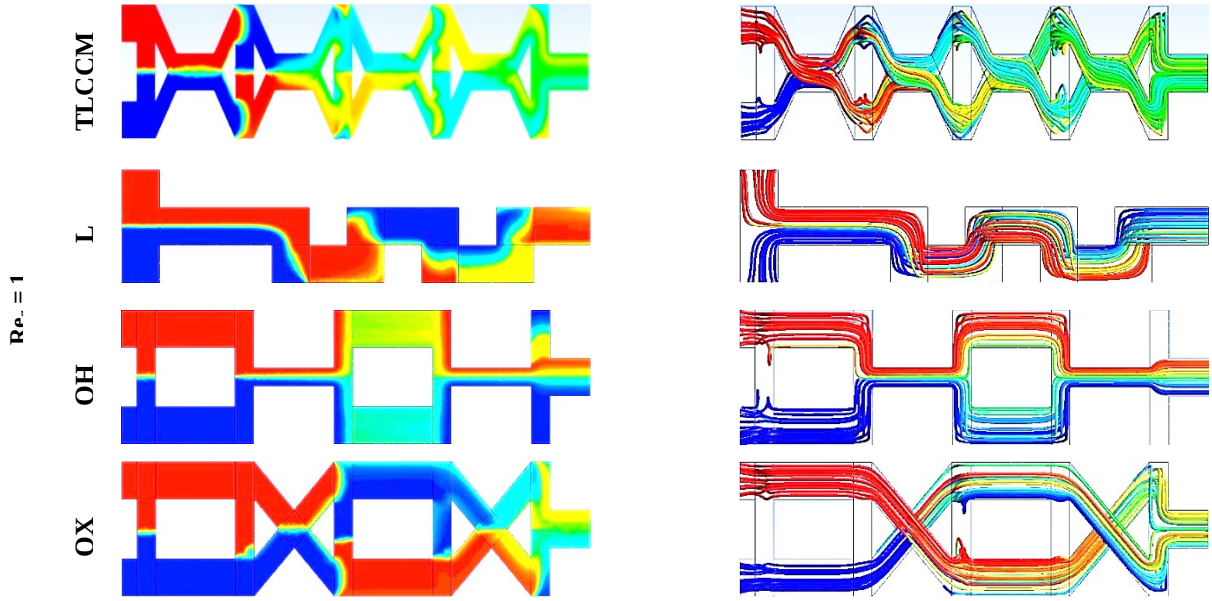

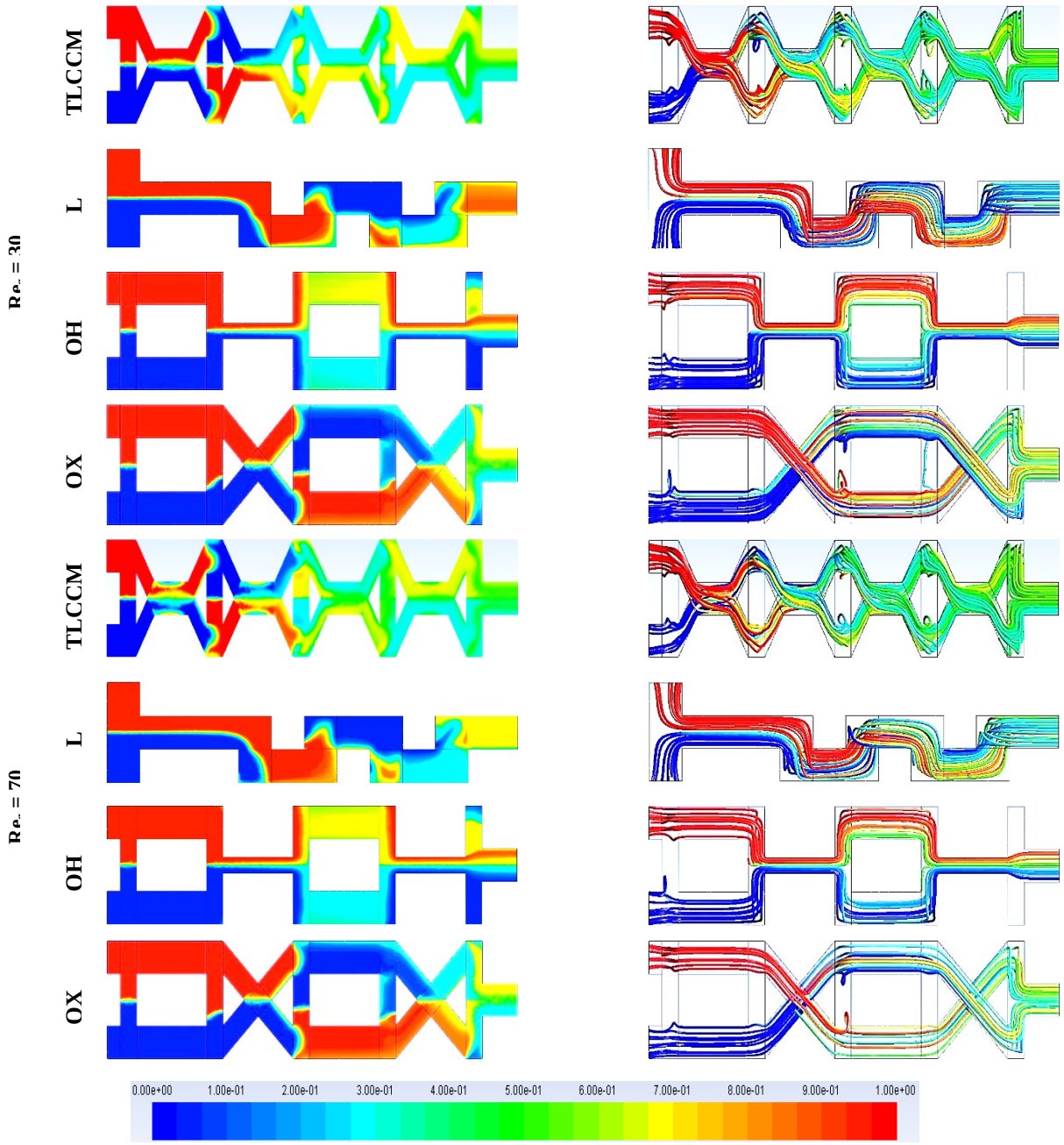

Fig. 12. Distributions of the mass fraction on the mid-plane (on the left side), and streamlines colored by the mass fraction (on the right side) of the proposed micromixers utilizing flow behavior index value of n = 0.49, and generalized Reynolds number values of (1, 30, and 70).

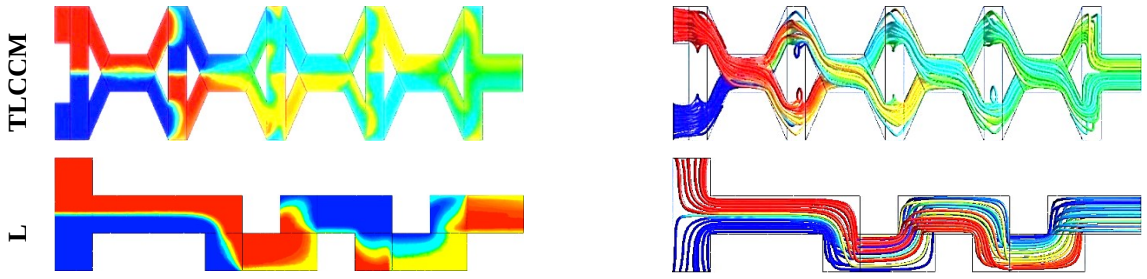

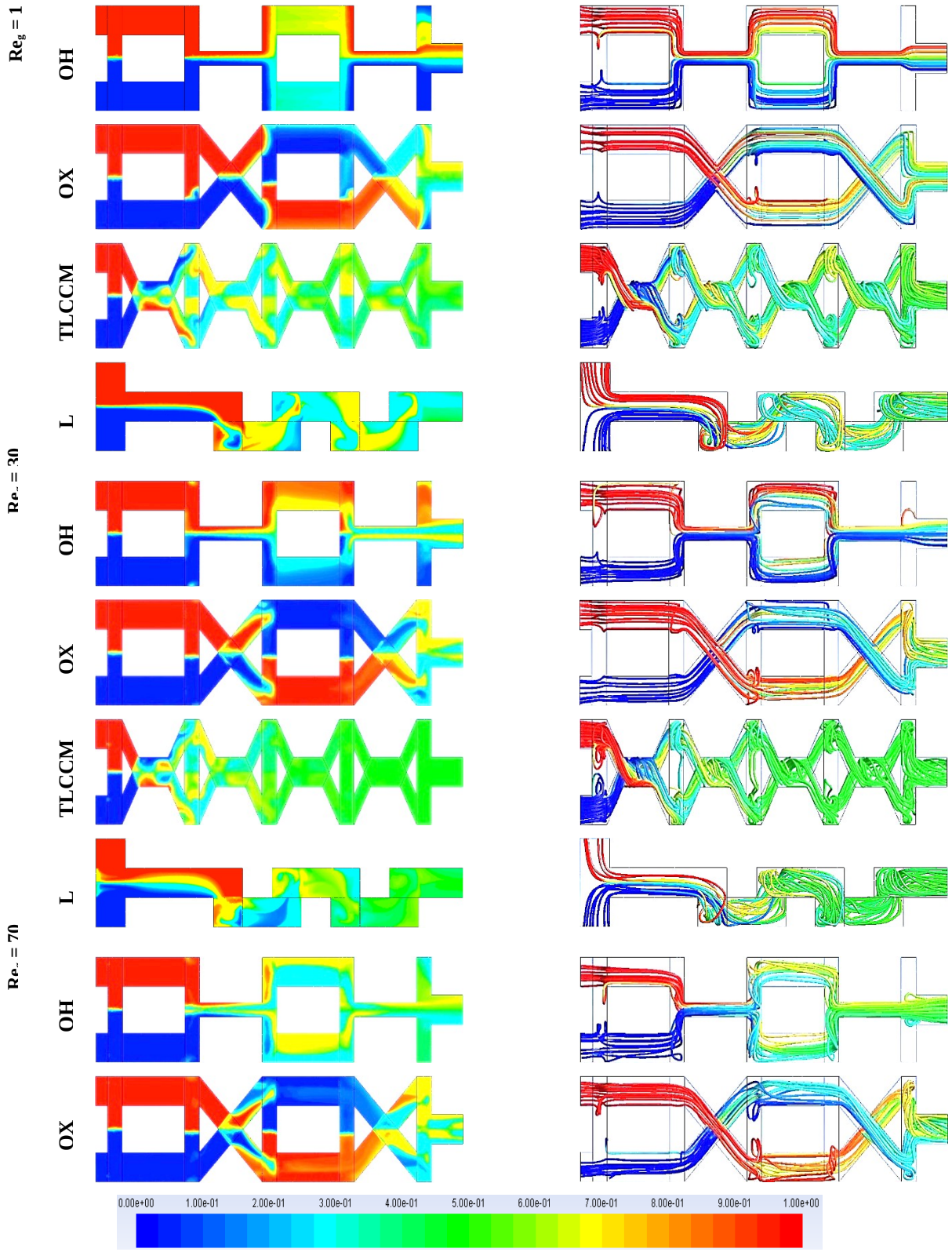

Fig. 13. Distributions of the mass fraction on the mid-plane (on the left side), and streamlines colored by the mass fraction (on the right side) of the proposed micromixers utilizing flow behavior index value of n = 1, and generalized Reynolds number values of (1, 30, and 70).

Fig. 14 and 15 illustrate the local progressions of the mixing degree D_m through the proposed micromixers for four values of Reynolds number (Re_g = 1, 15, 30, and 70), and two flow behavior index values (n=0.49 and n=1). Notably,

the curves corresponding to each micromixer are notably separated from one another, particularly for the TLCCM micromixer which has the elevated mixing efficiencies for both Newtonian and non-Newtonian fluids. From these figures, It's apparent that the mixing degree increases continuously through the TLCCM micromixer, for the two values of the flow behavior index. Indeed, the mixing degree reaches values greater than 50% and 80% for non-Newtonian fluids (n=0.49) and Newtonian fluids (n=1) respectively from the half of its length. Therefore, the values of the local mixing degree in different sections of the considered micromixers show the superiority of the TLCCM micromixer for the two considered flow behavior index and on the whole range of the generalized Reynolds number.

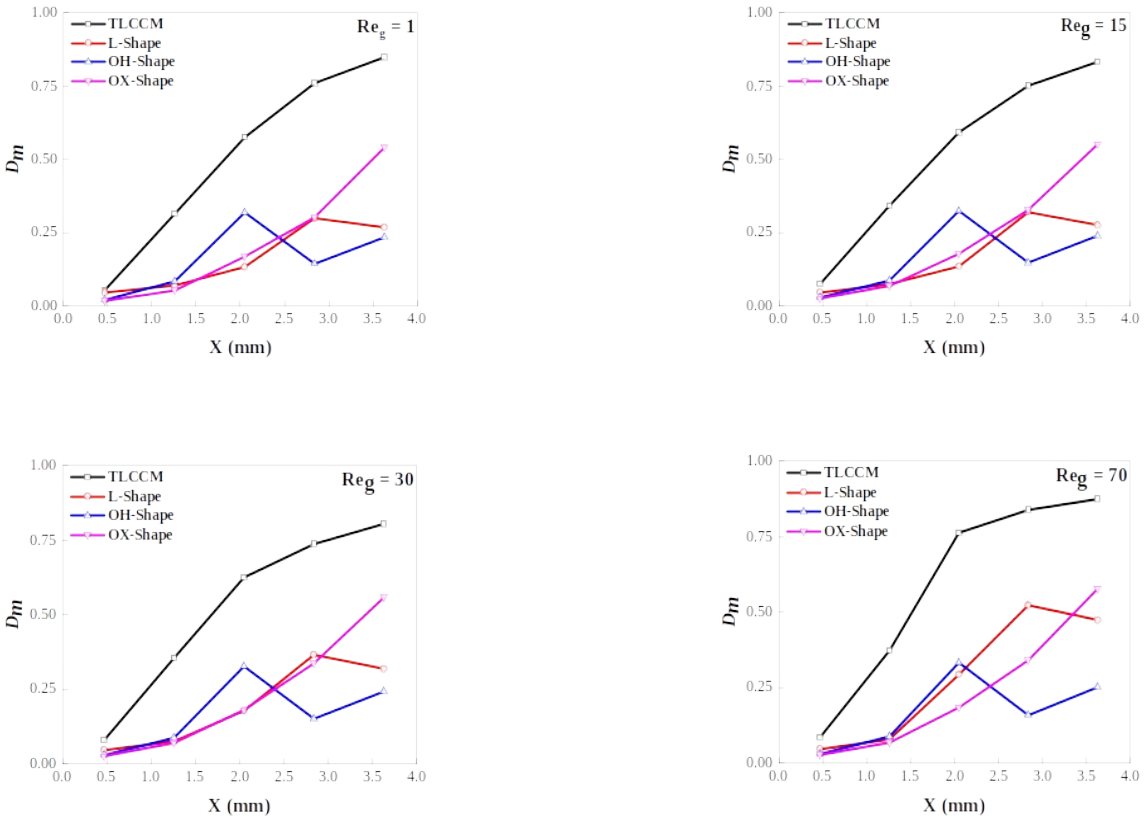

Fig. 14. Mixing degree evolutions through the proposed micromixers for generalized Reynolds numbers of (1, 15, 30, and 70), and flow behavior index of n = 0.49.

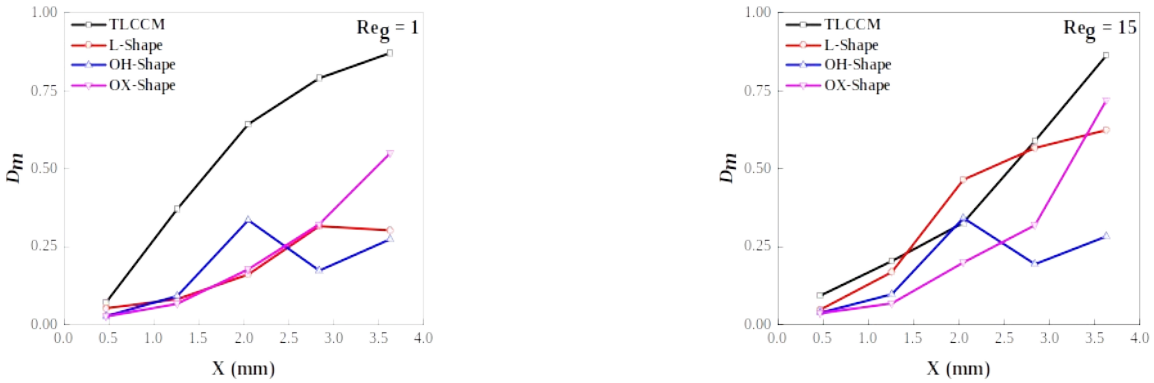

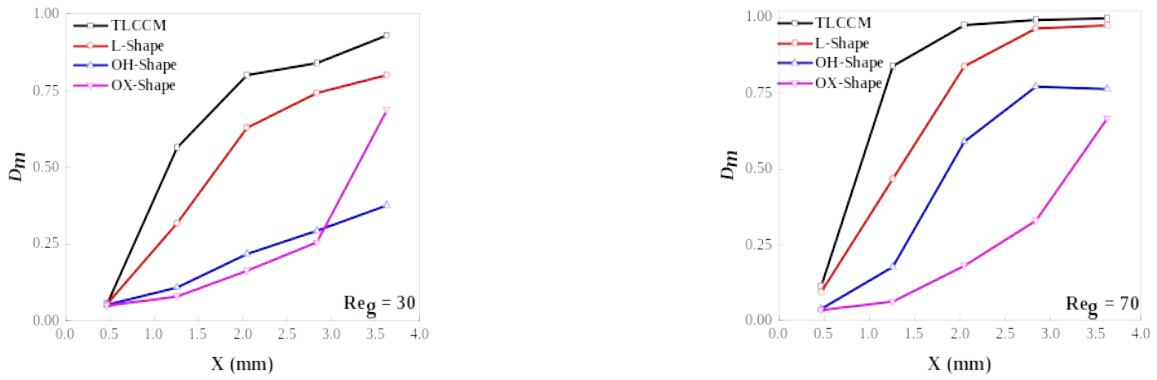

Fig. 15. Mixing degree evolutions through the proposed micromixers using generalized Reynolds numbers of (1, 15, 30, and 70), and flow behavior index of n = 1.

To assess and contrast the TLCCM micromixer efficiency with that of the other proposed micromixers. Fig. 16 illustrates a visual assessment of the mass fraction distributions at the outlet of the examined micromixers for two values of the flow behavior index (n=0.49 and n=0.93) and across all Reynolds number values (Re_g = 0.2 - 70). The mass fraction layouts illustrates the uniformity of the mixing which has been found using the TLCCM micromixer for the two values of flow behavior index (n=0.49 and n=0.93) and over the range of Reynolds numbers, this homogeneity matches the 0.5 mass fraction value, whereas the other micromixers exhibit poor mixing performance, particularly for fluids with a low flow behavior index (n = 0.49). For the TLCCM micromixer, the flow structure is completely different, this is visible at the exit plane where a homogeneous distribution of the mass fraction can be observed for the two flow regimes (diffusion and chaotic advection), and this structure shows clearly the intensity of the secondary flow generated in this micromixer. It is observed that the flow behavior index substantially affects the flow structure in every micromixer.

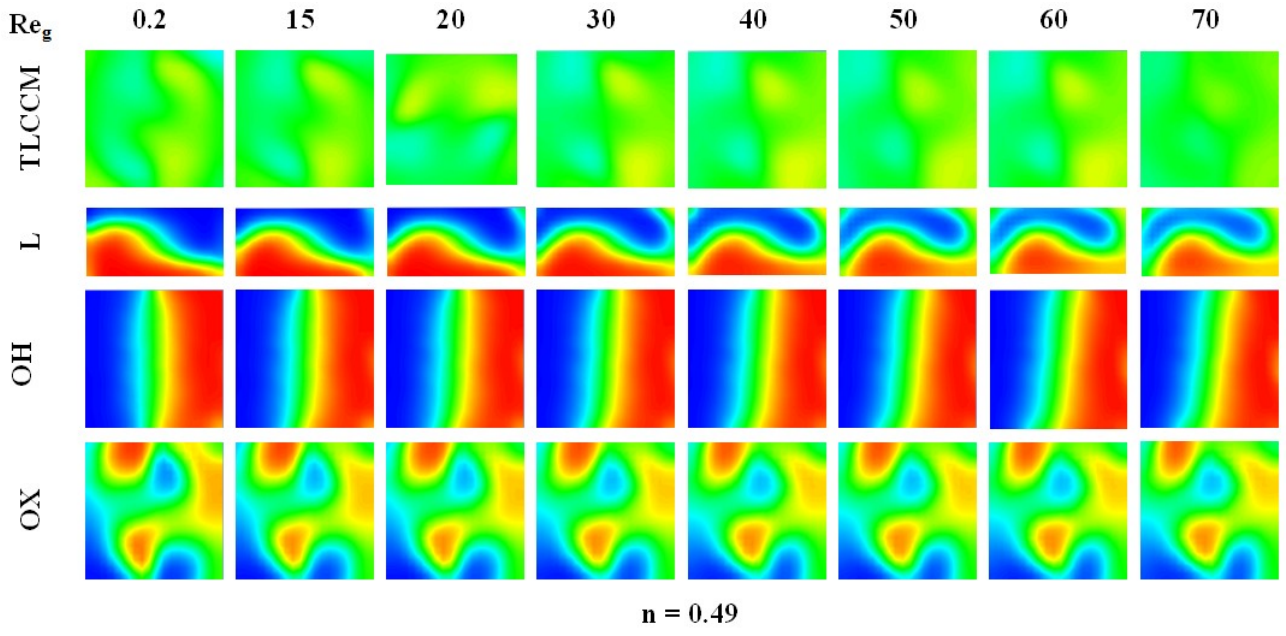

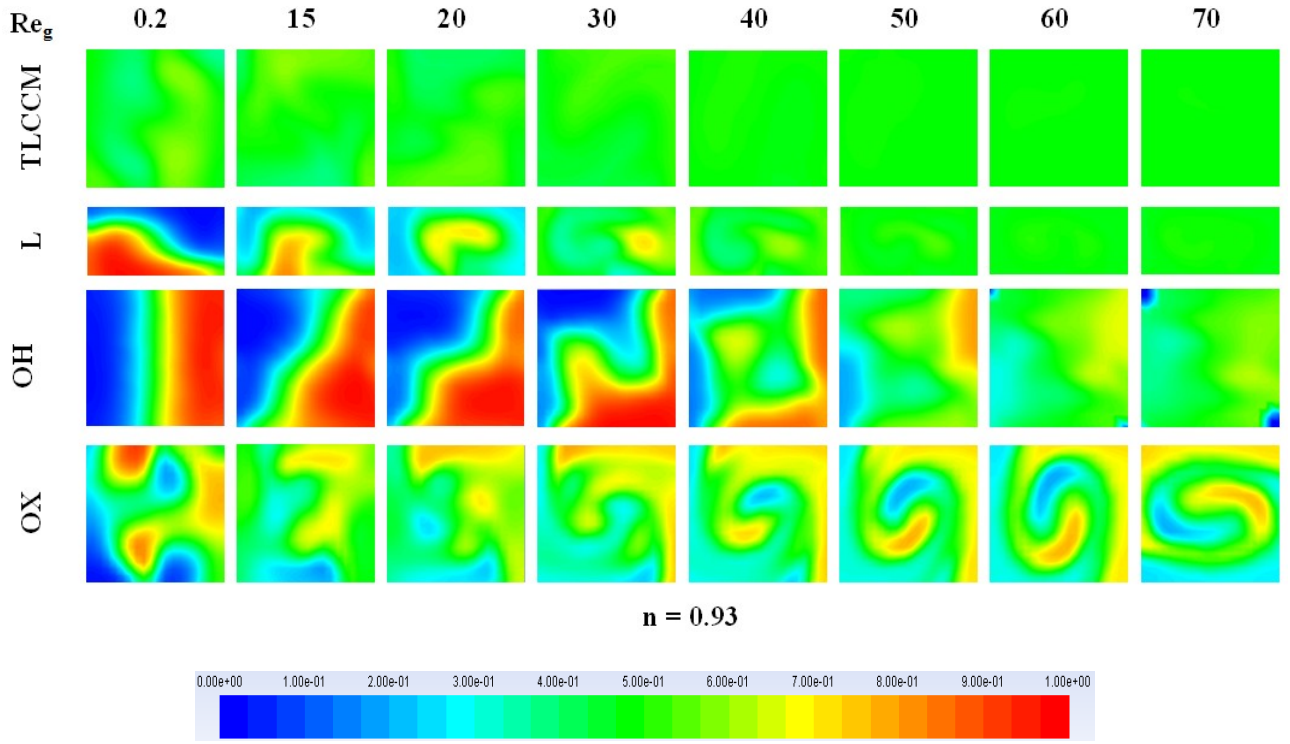

Fig. 16. Mass fraction distributions at the outlet of the proposed micromixers for the considered Reynolds number values with flow behavior index of 0.49 and 0.93.

A global view of the combined effect of the flow behavior index with the generalized Reynolds number makes it possible to examine in a clear way the effect of the micromixer geometries on the hydrodynamic mixing efficiencies. Fig. 17 illustrates the variation of the mixing degree in the proposed micromixers versus the generalized Reynolds number for the whole range of flow behavior index values. The TLCCM micromixer presents high values (more than 0.8) throughout the entire domain of the Reynolds number and whatever the flow behavior index, in particular for a very pseudoplastic fluid (n = 0.49) and low Reynolds numbers. For the other micromixers, It can be seen that the flow regime impacts the mixing degree where two regimes are distinguished: the molecular diffusion regime ($0.2 \leq \Re_g \leq 1$), and the chaotic advection regime ($\Re_g > 1$). Throughout the diffusion regime, the mixing degree of the considered micromixers achieves its maximum values concerning Newtonian fluids, and then it presents relatively lower values concerning non-Newtonian fluids. Particularly, the TLCCM micromixer demonstrates excellent mixing performance, exhibiting peak values for the two flow regimes, irrespective of the flow behavior index.

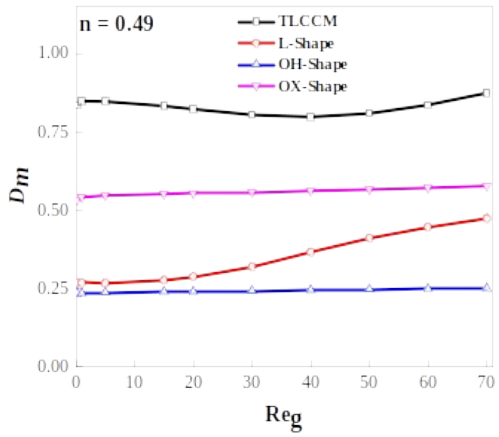

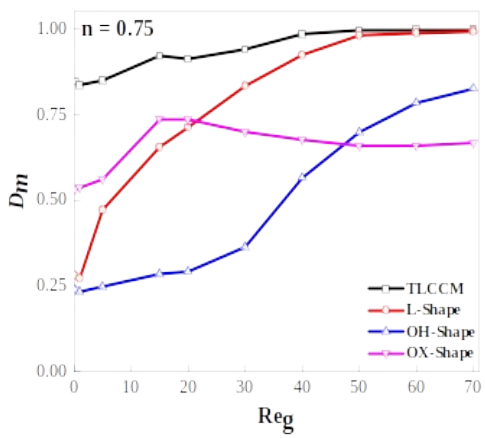

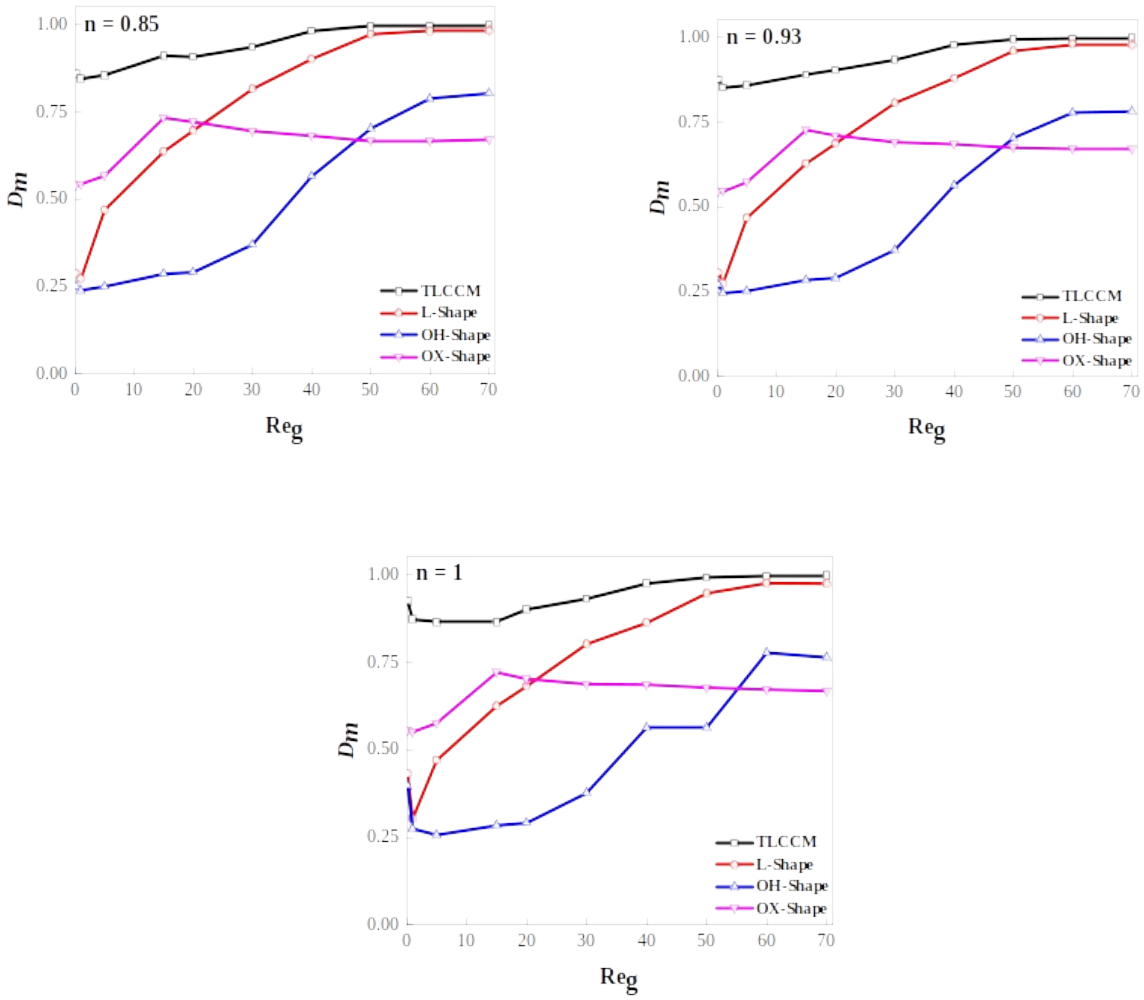

Fig. 17. Mixing degree variations against the generalized Reynolds numbers at the outlet of the considered micromixers for different flow behavior index values (0.49, 0.75, 0.85, 0.93 and 1).

To demonstrate the hydrodynamic mixing performance disparity between the TLCCM micromixer and the other suggested micromixers, it would be informative to graphically depict the mass fraction variations through the mid-line plane of the exit for all investigated micromixers, using a Reynolds number values range of (0.2; 20; 40; and 70) and two flow behavior index values of (n = 0.49 and n = 1). And to check mixing homogeneity obtained in each micromixer, the various curves of the mass fraction have been drawn as illustrated in Fig. 18. The mass fraction distribution curves exhibit deviations from each other, marked by notable fluctuations in the mass fraction values. These fluctuations have been remarked in the micromixers (L, OH and OX) for the entire generalized Reynolds number values. However, for the TLCCM micromixer, the mass fraction curves develop with weak fluctuations very near to the value of 0.5 for the considered Reynolds number values and the supposed flow behavior index, which illustrates the mixing uniformity obtained with this micromixer. This finding validates the earlier high mixing efficiencies achieved using the TLCCM micromixer.

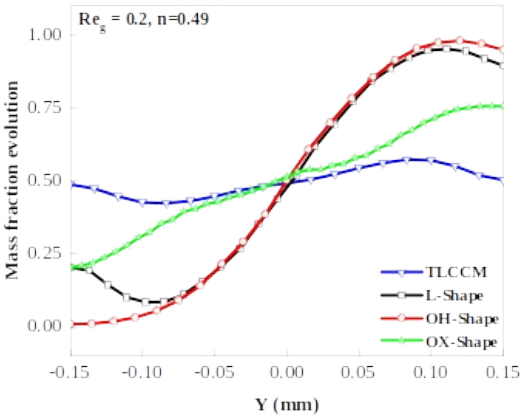
Re$_g$ = 0.2, n=0.49
Mass fraction evolution
Y (mm)
TLCCM
L-Shape
OH-Shape
OX-Shape

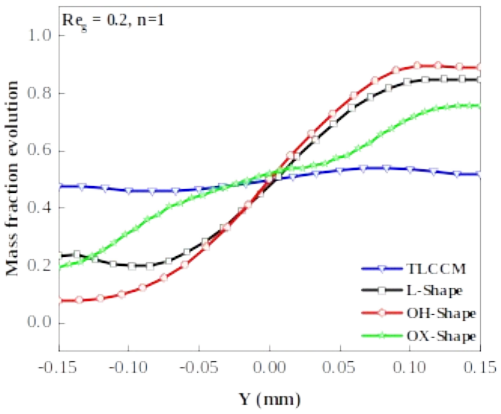
Re$_g$ = 0.2, n=1
Mass fraction evolution
Y (mm)
TLCCM
L-Shape
OH-Shape
OX-Shape

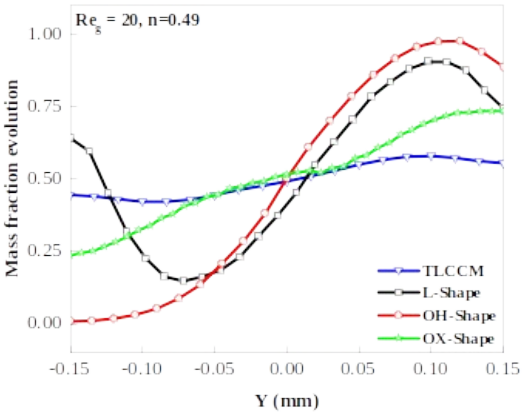
Re$_g$ = 20, n=0.49
Mass fraction evolution
Y (mm)
TLCCM
L-Shape
OH-Shape
OX-Shape

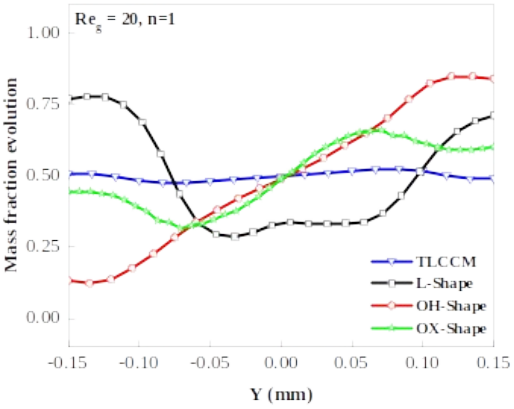
Re$_g$ = 20, n=1
Mass fraction evolution
Y (mm)
TLCCM
L-Shape
OH-Shape
OX-Shape

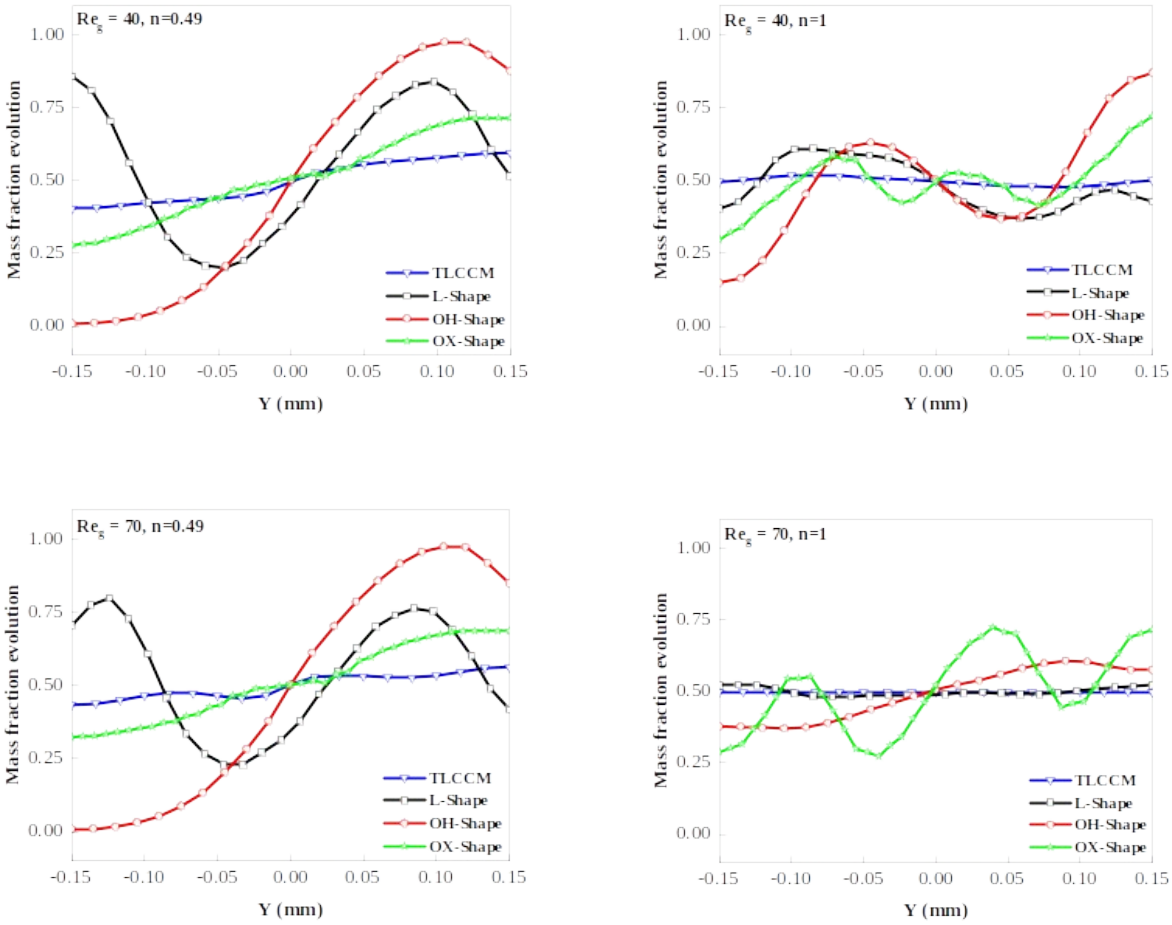

Fig. 18. Distributions of the mass fraction through the mid-line at the outlet of the studied micromixers with two flow behavior index values (0.49, and 1) and different Reynolds number values (0.2, 20, 40 and 70).

Fig. 19 shows the evolution of the shear rate along the meridian axis at the outlet of the considered micromixers for Re_g = 30, where the shear rate profile changes with the flow behavior index values for all the considered micromixers. It's clear that the shear rate has high values close to the walls of different micromixers for all the flow behavior index values, these values are very low in the middle of the exit planes and increase by approaching the walls. In comparison to the other micromixers, the TLCCM micromixer exhibits notably lower shear rate values for both Newtonian and non-Newtonian fluids, and as investigated previously (in Section 4-2), the decrease in the shear rate leads to improve the mixing capacity, which clarifies the high mixing performances of the TLCCM micromixer.

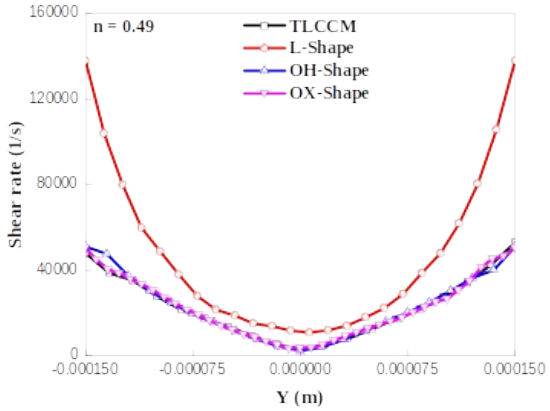
n = 0.49
TLCCM
L-Shape
OH-Shape
OX-Shape
Shear rate (1/s)
160000
120000
80000
40000
0
-0.000150
-0.000075
0.000000
0.000075
0.000150
Y (m)

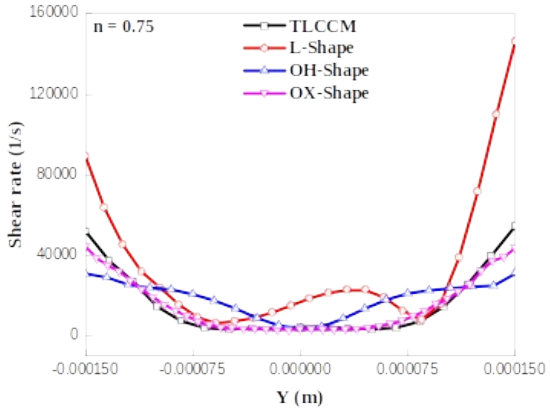
n = 0.75
TLCCM
L-Shape
OH-Shape
OX-Shape
Shear rate (1/s)
160000
120000
80000
40000
0
-0.000150
-0.000075
0.000000
0.000075
0.000150
Y (m)

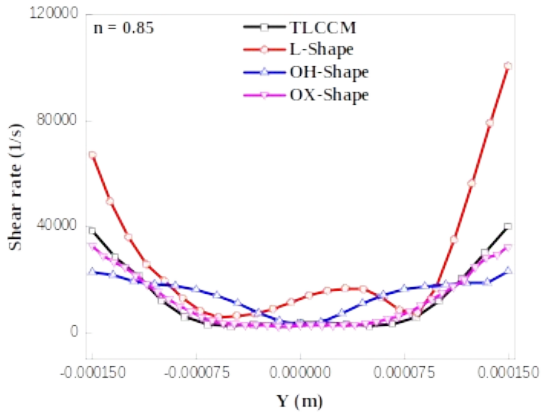
n = 0.85
TLCCM
L-Shape
OH-Shape
OX-Shape
Shear rate (1/s)
120000
80000
40000
0
-0.000150
-0.000075
0.000000
0.000075
0.000150
Y (m)

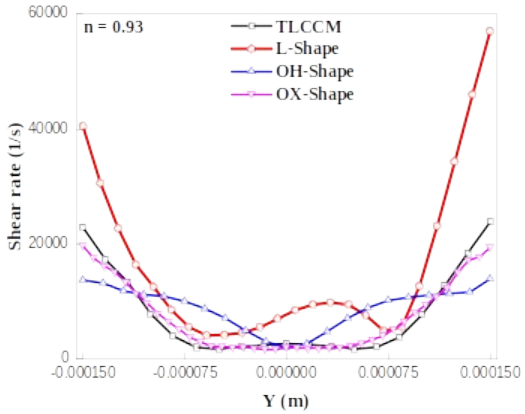
n = 0.93
TLCCM
L-Shape
OH-Shape
OX-Shape
Shear rate (1/s)
60000
40000
20000
0
-0.000150
-0.000075
0.000000
0.000075
0.000150
Y (m)

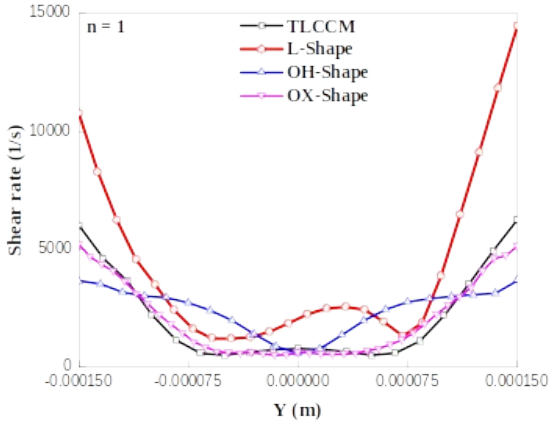

Fig. 19. Curves of the shear rate along the mid-line of the considered micromixers exit for $Re_g = 30$.

4.4. Mixing energy cost assessment

To select the optimal micromixer geometry, an additional variable is included to combine the two factors (mixing efficiency and pumping power) for evaluating micromixer performance. This parameter is based not solely on pressure losses but encompasses the overall required pumping power necessary to propel fluids through the micromixer (Mondal, et al.[71]). This is known by the mixing energy cost parameter "MEC" which is an important mixing variable, where a best micromixer is related to a minimal mixing energy cost, that translates into minimal pumping power with elevated mixing performances (Gidde, et al. [35]). The energy cost of mixing is established by (Javaid, et al. [37]):

$$MEC = \frac{Pumping\ power}{Mixing\ degree} = \frac{Q \times \Delta P}{D_m} \quad (22)$$

with Q represents the flow rate (m^3/s), while ΔP denotes the pressure losses : $\Delta P = P_{inlet} - P_{outlet}$.

The change in the mixing energy cost "MEC" for the micromixers under examination versus Reynolds number values is depicted in Fig. 20 for two extreme flow behavior index values (n = 0.49 and 1). It's apparent that this parameter escalates as the Reynolds number rises across all micromixers. This is attributed to the fact that hydrodynamic mixing conditions are influenced by the flow velocity, which in turn affects the flow rate. In general, the mixing energy cost exhibits the lowest values for low generalized Reynolds number values, such as $Re_g \leq 20$. Conversely, the mixing energy cost is notably influenced by the flow behavior index, as it escalates with a diminution in the flow behavior index (n=0.49). This relationship is rooted in the fluids rheological behavior: a higher flow behavior index leads to a reduced apparent viscosity, thereby enhancing fluid agitation. Consequently, the mixing degree experiences a significant boost, resulting in a lowered mixing energy cost. Worth noting is that all micromixers showcase exceedingly low mixing energy cost values, typically in the range of a few milliwatts.

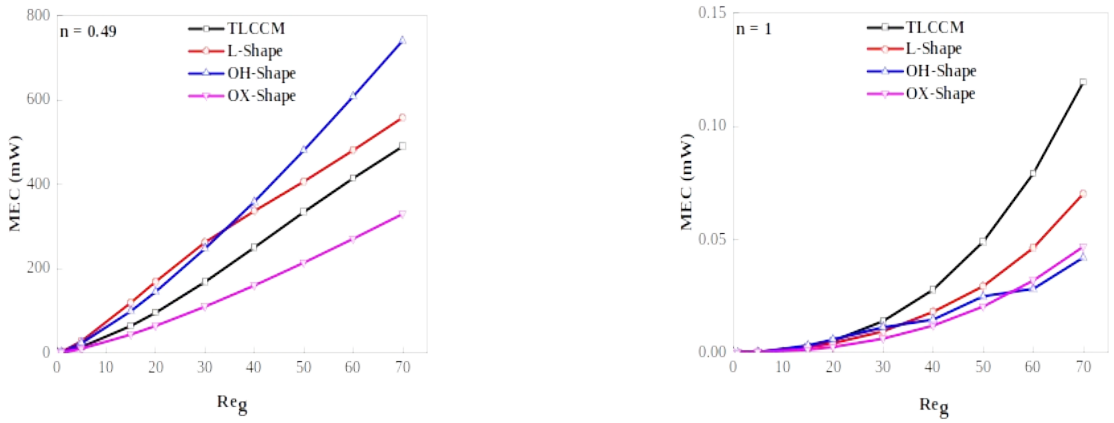

Fig. 20. Mixing energy costs comparison versus the generalized Reynolds numbers between the considered micromixers with two flow behavior index values (0.49, and 1).

5. Conclusions

The aim of this study is to contribute to the field of microfluidic systems particularly the modeling and the design of compact passive microdevices. A very efficient micromixer has been proposed which is characterized by Two Layer-Crossing Channels (TLCCM) with a very short length of 3.75 mm, which has shown best mixing performances and is operating in the laminar regime for Newtonian fluids. Numerical investigations were conducted by employing the ANSY-Fluent CFD code to assess the hydrodynamic mixing efficiencies of non-Newtonian pseudoplastic fluids in the suggested microdevices (TLCCM, L, OH, and OX). The performed validations show that the findings from the computational simulations are in good accordance with those of other computational previous works. It should be noted that the fluid rheological behavior exerts a substantial impact on the mixing performances. Newtonian fluids has low values of the apparent viscosity and shear rate, which leads to low velocities so an important residence time, therefore, the mixing becomes more and more homogeneous, it's the opposite of non-Newtonian fluids case. Besides, the impact of the residence time on the mixing performances was also examined by comparing the mixing degree and the flow rate versus the flow behavior index. The comparative study in terms of mixing degree, and mass fraction distributions, through and at the exit of the proposed micromixers permitted us to confirm the predominance of the TLCCM micromixer in the mixing of both Newtonian and non-Newtonian fluids, it has been illustrated that the evolutions of the mass fraction at the TLCCM micromixer exit revolve around 0.5 value, that signifies the situation of an ideal and uniform mixing. In addition, the TLCCM micromixer possesses the minimum mixing energy costs against the other studied micromixers investigated previously, that confirms the energy effectiveness of the TLCCM micromixer, especially at reduced values of Reynolds number. Overall, the TLCCM micromixer is very efficient, for hydrodynamic mixing with comparably low mixing energy cost.

Nonetheless, this investigation represents an important step towards designing a compact microdevice capable of achieving swift mixing at low values of Reynolds number. Furthermore, the investigation of mixing within the suggested micromixer can also be further expanded to non-Newtonian dilatant fluids, which can be supported by experiments.

6. References

[1] C.C. Domínguez, T. Gamse, Process intensification by the use of microdevices for liquid fractionation with supercritical carbondioxide, Chem. Eng. Res. Des. 108 (2016) 139–145.

[2] B. Morteza, N.M. Ashani, U. Azam, Active and passive micromixers: A comprehensive review, Chem Eng & Proces : Process Intensif. 147 (2020) 107771.

[3] E. Douroum, S. Laouedj, A. Benazza, A. Kouadri , Cooling of a surface with constant heat flow using a synthetic jet actuator, UPB Scientific Bulletin, Series D: Mechanical Engineering. 82(4) (2020) 293–306.

[4] A.G. Niculescu, C. Chircov, A.C. Bîrcă, A.M. Grumezescu, Fabrication and Applications of Microfluidic Devices: A Review, Inter J of Mol Sci. 22(4) (2021) 2011.

[5] J. Wang, G. Sui, V.P. Mocharla, R.J. Lin, M.E. Phelps, H.C. Kolb, H.R. Tseng, Integrated microfluidics for parallel screening of an in situ click chemistry library, Angew. Chem. Int. Ed. 45 (2006) 5276–5281.

[6] Y.N. Yang, H.I. Lin, J.H. Wang, S.C. Shiesh, G.B. Lee, An integrated microfluidic system for C-reactive protein measurement, Biosens. Bioelectron. 24 (2009)3091–3096.

[7] W.B. Lee, Y.H. Chen, H.I. Lin, S.C. Shiesh, G.B. Lee, An integrated microfluidic system for fast, automatic detection of C-reactive, Protein Sens. Actuators B:Chem. 157 (2011) 710–721.

[8] L. Wang, S. Ma, B. Yang, W. Cao, Xi. Han, Morphology-controlled synthesis of Ag nanoparticle decorated poly(o-phenylenediamine) using microfluidics and its application for hydrogen peroxide detection, Chem. Eng. J. 268(2015) 102–108.

[9] M. Ryu, J.A. Kimber, T. Sato, R. Nakatani, T. Hayakawa, M. Romano, C.Pradere, A.A. Hovhannisyan, S.G. Kazarian, J. Morikawa, Infraredthermo-spectroscopic imaging of styrene radical polymerization in microfluidics, Chem. Eng. J. 324 (2017) 259–265.

[10] E.S. Shanko, Y. van de Burgt, D.P. Anderson, M.J. den Toonder, Microfluidic Magnetic Mixing at Low Reynolds Numbers and in Stagnant Fluids, Micromachines. 10 (2019) 731.

[11] Z. Lu, J. McMahon, H. Mohamed, D. Barnard, T.R. Shaikh, C.A. Mannella, T. Wagenknecht, T.M. Lu, Passive microfluidic device for submillisecond mixing, *Sens. Actuators B. Chem.*144 (2010) 301–309.

[12] A. Cosentino, H. Madadi, P. Vergara, R. Vecchione, F. Causa, P.A. Netti, Anefficient planar accordion-shaped micromixer: from biochemical mixing tobiological application, Sci. Rep. 5 (2015) 17876.

[13] M. Cho, S. Chung, Y.T. Kim, J.H. Jung, D.H. Kim, T.S. Seo, A fully integratedmicrodevice for biobarcode assay based biological agent detection, Lab Chip15 (2015) 2744–2748.

[14] T. Han, L. Zhang, H. Xu, J. Xuan, Factory-on-chip. Modularised microfluidic reactors for continuous mass production of functional materials, Chem. Eng.J. 326 (2017) 765–773.

[15] H.S. Santana, J.L.S. Júnior, O.P. Taranto, Numerical simulation of mixing and reaction of Jatropha curcas oil and ethanol for synthesis of biodiesel in micromixers, Chem. Eng. Sci. 132 (2015) 159–168.

[16] J.N. Kuo, Y.H. Zhan, Microfluidic chip for rapid and automatic extraction of plasma from whole human blood, Microsyst. Technol. 21 (2015) 255–261.

[17] B. Swain, M.H. Hong, L. Kang, B.S. Kim, N.H. Kim, C.G. Lee, Optimization of CdSe nanocrystals synthesis with a microfluidic reactor and development of combinatorial synthesis process for industrial production, Chem. Eng. J. 308(2017) 311–321.

[18] W. Liu, Z. Xu, L. Sun, P. Guo, C. Zeng, C. Wang, L. Zhang,Polymerization-induced phase separation fabrication: a versatilemicrofluidic technique to prepare microfibers with various cross sectional shapes and structures, Chem. Eng. J. 315 (2017) 25–34.

[19] T.C. Kung, H. Gao, Y.C. Lee, N.Y. Wang, W. Dong, H.C. Ko, G. Wang, M.L. Fu, Microfluidic synthesis control technology and its application in drug delivery, bioimaging, biosensing, environmental analysis and cell analysis : Review, Chem. Eng. J. 399 (2020) 125748.

[20] K. Vimal, P. Marius, K.D. Nigam, Single-phase fluid flow and mixing in microchannels, Chem. Eng. Sci. 66(7) (2011) 1329–1373.

[21] M. Hashimoto, F. Barany, F. Xu, S.A. Soper, Serial processing of biologicalreactions using flow-through microfluidic devices: coupled PCR/LDR for thedetection of low-abundant DNA point mutations, Analyst 132 (2007)913–921.

[22] C.H. Lin, Y.N. Wang, L.M. Fu, Integrated microfluidic chip for rapid DNAdigestion and time-resolved capillary electrophoresis analysis,Biomicrofluidics 6 (2012) 012818.

[23] J.A. Lounsbury, A. Karlsson, D.C. Miranian, S.M. Cronk, D.A. Nelson, J. Li, D.M.Haverstick, P. Kinnon, D.J. Saul, J.P. Landers, From sample to PCR product inunder 45 minutes: a polymeric integrated microdevice for clinicalandforensic DNA analysis, Lab Chip 13 (2013) 1384–1393.

[24] A.S. Kastania, K. Tsougeni, G. Papadakis, E. Gizeli, G. Kokkoris, A. Tserepi, E.Gogolides, Plasma micro-nanotextured polymeric micromixer for DNApurification with high efficiency and dynamic range, Anal. Chim. Acta 942(2016) 58–67.

[25] C.Y. Lee, L.M. Fu, Recent advances and applications of micromixers, Sens. Actuators. B. 259 (2018) 677–702.

[26] J.N. Kuo, Y.S. Li, Centrifuge-based micromixer with three-dimensionalsquare-wave microchannel for blood plasma mixing, Microsyst. Technol. 23(2017) 2343–2354.

[27] J.N. Kuo, H.S. Liao, X.M. Li, Design optimization of capillary-drivenmicromixer with square-wave microchannel for blood plasma mixing,Microsyst. Technol. 23 (2017) 721–730.

[28] Y. Okubo, T. Maki, F. Nakanishi, T. Hayashi, K. Mae, Precise control of polymer particle properties using droplets in the microchannel, Chem. Eng. Sci. 65(1) (2010) 386–391.

[29] Y.T. Chen, K.H. Chen, W. F. Fang, S.H. Tsai, J.M. Fang, J.T. Yang, Flash synthesis of carbohydrate derivatives in chaotic microreactors, Chem. Eng. J. 174(1) (2011) 421–424.

[30] Y. Gambin, C. Simonnet, V. VanDelinder, A. Deniz, A. Groisman, Ultrafast microfluidic mixer with three - dimensional flow focusing for studies of biochemical kinetics, Lab Chip 10 (2010) 598–6097.

[31] S.H. Santana, S.D. Tortola, L.J. Silva, P.O. Taranto, Biodiesel synthesis in micromixer with static elements, Ener. Conv. and Man. 141 (2017) 28–39.

[32] H. Aref, Stirring by chaotic advection, J. Fluid. mech. 143 (1984) 1–21.

[33] A. Banerjee, K.A. Nayak, B. Weigand, Enhanced mixing and flow reversal in a modulated microchannel, Int. J. of Mech. Sci. 155 (2019) 430–439.

[34] Y.C. Lee, L.C. Chang, N.Y. Wang, F.L. Ming, Microfluidic Mixing: A Review, Int. J. Mol. Sci. 12 (2011) 3263–3287.

[35] R.R. Gidde, P.M. Pawar, Flow feature and mixing performance analysis of RB-TSAR and EB-TSAR micromixers, Microsys. Tech. 26 (2020) 517–530.

[36] R.R. Gidde, Concave wall-based mixing chambers and convex wall-based constriction channel micromixers, Int. J. of Env. Anal. Chem. 1(23) (2019) 0306–7319.

[37] U.M. Javaid, A.T. Cheema, W.C. Park, Analysis of passive mixing in a serpentine microchannel with sinusoidal side walls, Micromachines. 9(1) (2018) 1–15.

[38] H. Aref, The development of chaotic advection, Phys. Fluids. 14(04) (2002) 1315–1325.

[39] E. Tripathi, P.K. Patowari, S. Pati, Numerical investigation of mixing performance in spiral micromixers based on Dean flows and chaotic advection, Chem. Eng. Proc: Proc. Int. 169 (2021) 108609.

[40] W. Raza, N. Islam, A. Samad, Design and analysis of a novel Bi-layer curved serpentine chaotic micromixer for efficient mixing, Chem. Eng. Proc: Proc. Int. 183 (2023) 109246.

[41] C. Srisamran, S. Devahastin, Numerical simulation of flow and mixing behavior of impinging streams of shear-thinning fluids, Chem. Eng. Sci. 61 (2006) 4884–4892.

[42] A. Afzal, K-Y. Kim, Flow and mixing analysis of non-Newtonian fluids in straight and serpentine microchannels, Chem. Eng. Sc. 116 (2014) 263–274.

[43] S.B. Islami, M. Khezerloo, R. Gharraei, The effect of chaotic advection on mixing degree and pressure drop of non-Newtonian fluids flow in curved micromixers, J. Braz. Soc. Mech. Sci. 10 (2016) 1–19.

[44] D.A. Fallah, M. Raad, S. Rezazadeh, J. Habib, Increment of mixing quality of Newtonian and non-Newtonian fluids using T-shape passive micromixer: numerical simulation. Microsys. Tech. 27 (2021) 189–199.

[45] B. Talebjedi , M. Ghazi , N. Tasnim , S. Janfaza , M. Hoorfar, Performance optimization of a novel passive T-shaped micromixer with deformable baffles, Chem. Eng. Proc: Proc. Int. 163 (2021) 108369.

[46] D. Gu, T. Yang, L. Xie, Mixing Characteristics of Shear-Thinning Fluids in a Fractal Perforating Impeller Stirred Reactor, Ind. & Eng. Chem. Res. 62(28) (2023) 11194–11205.

[47] J. Wang, S. Ma, P. Chen, Z. Li, Z. Gao, J.J. Derksen, Mixing of miscible shear-thinning fluids in a lid-driven cavity, Chin. J. of Chem. Eng. 58 (2023) 112–123.

[48] S. Wang, P. Wang, J. Yuan, J. Liu, Q. Si, D. Li, Simulation Analysis of Power Consumption and Mixing Time of Pseudoplastic Non-Newtonian Fluids with a Propeller Agitator. Energies. 15 (13) (2022) 4561.

[49] Z.G. Kharaji, V. Kalantar, M. Bayareh, Mixing enhancement in an acousto-inertial microfluidic system, Chem. Eng. Proc: Proc. Int. 191 (2023) 109473.

[50] J. Ramírez-Muñoz, V.E. Márquez-Baños, J. Alvarez-Vega, R. Mompremier, J. Gómez Núñez, R. Guadarrama-Pérez, Hydrodynamics performance of Newtonian and shear-thinning fluids in a tank stirred with a high shear impeller: Effect of liquid height and off-bottom clearance, Chem. Eng. Res. Des. 192 (2023) 44–54.

[51] T. Niederkorn, J. Ottino, Chaotic mixing of shear-thinning fluids, AIChE. J. 40(11) (1994) 1782–1793.

[52] P.D. Anderson, O.S. Galaktionov, G.M. Peters, F.N. van de Vosse, H.H. Meijer, Mixing of non-Newtonian fluids in time-periodic cavity flows, J. Nonnewtonian. Fluid. Mech. 93 (2000) 265–286.

[53] G. Ascanio, S. Foucault, P.A. Tanguy, Time-periodic mixing of shear-thinning fluids, Chem. Eng. Res. Design. 82(A9) (2004) 1199–1203.

[54] C.C. Cho, C.L. Chen, C.K. Chen, Mixing enhancement of electrokinetically-driven non-Newtonian fluids in microchannel with patterned blocks, Chem. Eng. J. 191 (2012) 132–140.

[55] R.T. Tsai, C.Y. Wu, C.Y. Chang, M.Y. Kuo, Mixing Behaviors of Shear-Thinning Fluids in Serpentine Channel Micromixers, Int. J. Mech. Aero. Ind. Mech. Man. Eng. 9(7) (2015) 1329–1335.

[56] R. Shamsoddini, M. Sefid, R. Fatehi, Incompressible SPH modeling and analysis of non-Newtonian power-law fluids, mixing in a microchannel with an oscillating stirrer, J. Mech. Sci. Tech. 30(1) (2016) 307–316.

[57] S.B. Islami, M. Khezerloo, Enhancement of Mixing Performance of Non-Newtonian Fluids using Curving and Grooving of Microchannels, J. App. Fluid. Mech. 10(1) (2017) 127–141.

[58] G. Kunti, A. Bhattacharya, S. Chakraborty, Analysis of micromixing of non-Newtonian fluids driven by alternating current electrothermal flow, J. Nonnewtonian. Fluid. Mech. 247 (2017) 123–131.

[59] A. Bordbar, A. Taassob, R. Kamali, Diffusion and Convection Mixing of Non-Newtonian Liquids in an Optimized Micromixer, The Canadian. J. of Chem. Eng. 96(8) (2017) 1829–1836.

[60] A.S. Lobasov, A.V. Minakov, Y.V. Rudyak, Flow Modes of Non-Newtonian Fluids with Power-Law Rheology in a T-Shaped Micromixer, Theo. Foun. of Chem. Eng. 52(3) (2018) 393–403.

[61] M. He, W. Li, M. Zhang, J. Zhang, Numerical investigation on the efficient mixing of overbridged Split And Recombine micromixer at low Reynolds number, Micro. Tech. 25(9) (2019) 3447–3461.

[62] A. Kouadri, Y. Lasbet, M. Makhlouf, High mixing performances of shear-thinning fluids in two-layer crossing channels micromixer at very low Reynolds numbers, J. Mech. Eng. Sci. 13(4) (2019) 5938–5960.

[63] A. Kouadri, E. Douroum, Y. Lasbet, T.T. Naas, S. Khelladi, M.Makhlouf. Comparative study of mixing behaviors using non-Newtonian fluid flows in passive micromixers, Int. J. Mech. Sci. 201 (2021) 106472.

[64] A. Kouadri, E. Douroum, S. Khelladi, Parametric study of the Crossing elongation effect on the mixing performances using short Two-Layer Crossing Channels Micromixer (TLCCM) geometry, Chem. Eng. Res. Design. 158 (2020) 33–43.

[65] E. Douroum, S. Laouedj, A. Kouadri, T.T. Naas, S. Khelladi, A. Benazza, High hydrodynamic and thermal mixing performances of efficient chaotic micromixers: A comparative study, Chem. Eng. & Proc: Proc. Int. 164(108394) (2021) 1–19.

[66] E. Douroum, A. Kouadri, A. Tahiri, M. Brihmat, S. Khelladi, Hydrodynamic and Kinematic Study to Analyze the Mixing Efficiency of Short Passive Micromixers, Ind. Eng. Chem. Res. 61 (17) (2022) 5994−6009.

[67] T. Das, S. Chakraborty, Recent trends and future challenges, Biomicrofluidics. Sadhana. 34(4) (2009) 573–590.

[68] H. Fellouah, C. Castelain, A. Ould-El-Moctar, H. Peerhossaini, The Dean instability in power-law and Bingham fluids in a curved rectangular duct, J. Nonnewtonian. Fluid. Mech. 165 (2010) 163–173.

[69] F.T. Pinho, J.H. Whitelaw, Flow of non-Newtonian fluids in a pipe, J. Nonnewtonian. Fluid. Mech. 34 (1990) 129–144.

[70] F. Delplace, J.C. Leuliet, Generalized Reynolds number for the flow of power law fluids in cylindrical ducts of arbitrary cross-section, Chem. Eng. J. 56 (1995) 33–37.

[71] B. Mondal, K.S. Mehta, K.P. Patowari, S. Pati, Numerical study of mixing in wavy micromixers: comparison between raccoon and serpentine mixer, Chem. Eng. Proc: Proc. Int. 136 (2019) 44–61.